

1 **Future water storage changes over the Mediterranean, Middle East, and North Africa in**
2 **response to global warming and stratospheric aerosol intervention**

3 **Abolfazl Rezaei^{1,2}, Khalil Karami³, Simone Tilmes⁴, John C. Moore⁵**

4 ¹ Department of Earth Sciences, Institute for Advanced Studies in Basic Sciences (IASBS), Zanjan
5 45137-66731, Iran. arezaei@iasbs.ac.ir; abolfazlrezaei64@gmail.com.

6 ² Center for Research in Climate Change and Global Warming (CRCC), Institute for Advanced Studies
7 in Basic Sciences (IASBS), Zanjan 45137-66731, Iran

8 ³ Institut für Meteorologie, Stephanstraße 3, 04103 Leipzig, Germany. khalil.karami@uni-leipzig.de

9 ⁴ National Center for Atmospheric Research, Boulder, CO, USA. tilmes@ucar.edu

10 ⁵ Arctic Centre, University of Lapland, Rovaniemi, 96101, Finland. john.moore.bnu@gmail.com

11
12 **Abstract**

13 Water storage plays a profound role in the lives of people across the Middle East and North Africa
14 (MENA) as it is the most water stressed region worldwide. The lands around the Caspian and
15 Mediterranean Seas are simulated to be very sensitive to future climate warming. Available water
16 capacity depends on hydroclimate variables such as temperature and precipitation that will depend
17 on socioeconomic pathways and changes in climate. This work explores changes in both the mean
18 and extreme terrestrial water storage (TWS) under an unmitigated greenhouse gas (GHG) scenario
19 (SSP5-8.5) and stratospheric aerosol intervention (SAI) designed to offset GHG-induced warming
20 above 1.5 °C and compares both with historical period simulations. Both mean and extreme TWS are
21 projected to significantly decrease under SSP5-8.5 over the domain, except for the Arabian Peninsula,
22 particularly in the wetter lands around the Caspian and Mediterranean Seas. Relative to global
23 warming, SAI partially ameliorates the decreased mean TWS in the wet regions while it has no
24 significant effect on the increased TWS in drier lands. In the entire domain studied, the mean TWS is
25 larger under SAI than pure greenhouse gas forcing, mainly due to the significant cooling, and in turn,
26 a substantial decrease of evapotranspiration under SAI relative to SSP5-8.5. Changes in extreme
27 water storage excursions under global warming are reduced by SAI. Extreme TWS under both future
28 climate scenarios are larger than throughout the historical period across Iran, Iraq, and the Arabian
29 Peninsula, but the response of the more continental eastern North Africa (NA) hyper-arid climate is
30 different from the neighboring dry lands. In the latter case, we note a reduction in the mean TWS
31 trend under both GHG and SAI scenarios, with extreme TWS values also showing a decline compared
32 to historical conditions.

33 **Keywords:** Mean and extreme water storage; SSP5-8.5; Stratospheric Aerosol Intervention; Global
34 warming; MENA region, Caspian and Mediterranean Seas

35

36 **500-character non-technical text**

37 Water storage (WS) plays a profound role in the lives of people in the Middle East and North Africa
38 and Mediterranean climate “hot spots”. Simulated is WS changed by greenhouse gas (GHG) warming
39 with and without stratospheric aerosol intervention (SAI). WS significantly increases in the Arabian
40 Peninsula and decreases around Mediterranean under GHG. While SAI partially ameliorates the GHG
41 impacts, ~~P~~projected WS increases in dry regions and decreases in wet areas relative to the present
42 climate.

43

44 **1. Introduction**

45 The Middle East and North Africa (MENA), with 6% of the world’s population, are currently among
46 the most water-stressed regions worldwide (Fragaszy et al., 2020). The dry climate, intensifying
47 droughts, increasing population, and water over-extraction particularly across the Middle East
48 (World Bank, 2017), make it home to 12 of the 17 most water-stressed countries on the planet
49 (Hofste et al., 2019). Water availability is crucial for sanitation (Reiter et al., 2004), economic activity
50 (UNESCO, 2003), ecosystems (Shiklomanov and Rodda, 2003), and hydrological systems (Mooney et
51 al., 2005).

52

53 The MENA region has the largest expected economic losses from climate-related water scarcity,
54 robustly estimated at 6–14 % of Gross Domestic Product (GDP) by 2050 (World Bank, 2017). MENA’s
55 terrestrial water storage (TWS) is being intensively extracted and may act as a flashpoint for conflict
56 (Famiglietti, 2014). TWS incorporates all water on the land surface (snow, ice, water stored in the
57 vegetation, river, and lake water) and in the subsurface (soil moisture and groundwater). Beyond
58 anthropogenic activities, natural climate variability such as drought frequency affects water storage
59 and agriculture, which then impacts food security (Fragaszy et al., 2020). The Middle East is
60 especially prone to severe and sustained droughts due to its location in the descending limb of the
61 Hadley circulation and associated dry and semiarid climate (Barlow et al., 2016). The 1998-2012 14-
62 year period was the worst drought in the past 900 years (Cook et al., 2016). Because the saturated
63 vapor pressure of air is largely controlled by temperature, any change in temperature, as well as
64 precipitation, substantially affects (Konapala et al., 2020; Ajjur and Al-Ghamdi, 2021; Hobeichi et al.,
65 2022) the water storage capacity available to supply the increasing water demand in the region (Lian,

66 2021). The MENA region, having both low precipitation and high evaporation, is very vulnerable to
67 climate change (Giorgi, 2006; Lelieveld et al., 2012; Tabari and Willems, 2018; Zittis et al., 2019).
68 MENA water storage is therefore particularly sensitive to any perturbation of the water cycle
69 imposed by global warming.

70 ~~Although MENA's adjacent densely populated region, the Mediterranean, has a better water storage~~
71 ~~state, it is projected to substantially suffer from reduced water availability under future GHG climate~~
72 ~~scenarios (Lionello et al., 2006). This is due to both projected significant decreases in rainfall~~
73 ~~(Azzopardi et al., 2020) and large increases in demand for irrigation water by the end of the 21st~~
74 ~~century (Fader et al. 2016).~~

75
76 ~~If global mean surface temperature rises to exceed 1.5 °C above the preindustrial mean temperature,~~
77 ~~severe global consequences, and societal problems can be expected (Masson-Delmotte, 2022). Solar~~
78 ~~radiation modification (SRM), a form of intervention to cool the climate by reflecting sunlight, has~~
79 ~~been proposed as a potential method of limiting global temperature rises and the associated impacts~~
80 ~~of increased GHG emissions. SRM is likely the only way to keep or reduce surface temperatures to~~
81 ~~1.5C given the reality of the GHG mitigation measures that have been agreed to date (MacMartin et~~
82 ~~al., 2022). Simulations have shown a 2% decrease in total solar irradiance roughly offsets global~~
83 ~~warming due to a doubling of CO₂ concentrations, and continuous injections of 10–18 Tg SO₂ would~~
84 ~~lead to a cooling of about 1 °C after several years (WMO, 2022). This is consistent with observed~~
85 ~~surface cooling after large volcanic eruptions, such as the 1991 Mt Pinatubo eruption which produced~~
86 ~~cooling of about 0.3 °C over a 2–3 year period (e.g., IPCC, 2021).~~

87 GHG warming has already adversely affected water resources in the MENA region (Wang et al., 2018)
88 and is simulated to intensify water competition between states (Arnell, 1999) in the future. Although
89 global warming is expected to increase precipitation and soil moisture across MENA (Cook et al.,
90 2020), it will decrease runoff and groundwater recharge by larger amounts (Milly et al., 2005;
91 ~~Shaban, 2008~~; Suppan et al., 2008; ~~Shaban 2008~~). Using ~~the~~ GHG emission scenario A1B simulated by
92 nine CMIP3-class climate models, Droogers et al. (2012) projected that 22-% of the future annual
93 water shortage, 199 km³ in 2050 in MENA, will be due to global warming. 17 global climate models
94 from Coupled Model Intercomparison Project Phase 6 (CMIP6) under SSP5-8.5 simulate a significant
95 increase in precipitation (+0.05 to 0.3 ± 0.1 mm day⁻¹) over South-Eastern Saharan Desert in NA by
96 the end of the century (Aridal et al., 2023). They also projected that the total soil moisture would
97 increase over Southern Saharan Desert under the SSP5-8.5 (6 to 20%) and SSP2-4.5 (4 to
98 14%). Based on TWS data from eight global climate models participating in CMIP6, a broad part of

99 the dry MENA region tends to be wetter under SSP5-8.5 over 2071-2100 (Xiong et al., 2022). GHG-
100 driven groundwater storage depletion in the Middle East during the 21st century will far exceed that
101 during the 20th century due to the increased evapotranspiration (ET) and reduced volume of
102 snowmelt (Wu et al., 2020).

103

104 Although MENA's adjacent densely populated region, the Mediterranean, has a better water storage
105 state, it is projected to substantially suffer from reduced water availability under future GHG climate
106 scenarios (Lionello et al., 2006). This is due to both projected significant decreases in rainfall
107 (Azzopardi et al., 2020) and large increases in demand for irrigation water by the end of the 21st
108 century (Fader et al., 2016). The precipitation and water availability in the Mediterranean region, to
109 the northwest of the MENA, is also projected to be highly sensitive to global warming, particularly
110 regarding water availability (Lionello et al., 2006), having the largest differences in the water
111 availability between 1.5 and 2°C warming scenarios globally (Schleussner et al., 2016). Global
112 warming decreases Mediterranean groundwater recharge according to simulations under the IPCC
113 A2 and B2 scenarios simulated using ECHAM4 and HadCM3 models (Döll and Flörke, 2005). Runoff
114 is decreased by 10-30% according to 12 models such as CCSM3, and ECHAM5/MPI-OM (Milly et al.,
115 2005), and soil moisture z-scores (obtained by taking the difference from the average and then
116 dividing it by the standard deviation of the time series from the baseline period) by -1 to -4 in warm
117 seasons according to simulations under SSP1-2.6, SSP2-4.5, SSP3-7.0, and SSP5-8.5 (Cook et al.,
118 2020). Water availability in turn is lowered by 8-28% for a warming of 2 °C as simulated by 11
119 CMIP5-class models by Schleussner et al., (2016). Likewise, Döll et al. (2018) found a strong drying
120 in the Mediterranean region under global warming since the largest precipitation decreases
121 worldwide were simulated in this region under SSP1-2.6, SSP2-4.5, SSP3-7.0, and SSP5-8.5 scenarios
122 (Cook et al., 2020). CMIP5 model results also confirm that the global warming (RCP2.6 and RCP6.0)
123 substantially decreases the TWS in the Mediterranean by the mid- (2030-2059) and late- (2070-
124 2099) twenty-first century (Pokhrel et al., 2021).

125

126 If global mean surface temperature rises to exceed 1.5 °C above the preindustrial mean temperature,
127 severe global consequences, and societal problems can be expected (Masson-Delmotte, 2022). Solar
128 radiation modification (SRM), a form of intervention to cool the climate by reflecting sunlight, has
129 been proposed as a potential method of limiting global temperature rises and the associated impacts
130 of increased GHG emissions. SRM may be the only way to keep or reduce surface temperatures to 1.5
131 °C given the reality of the GHG mitigation measures that have been agreed upon to date (MacMartin

132 [et al., 2022](#)). Simulations have shown a 2% decrease in total solar irradiance roughly offsets global
133 [warming due to a doubling of CO₂ concentrations, and continuous injections of 10-18 Tg SO₂ per year](#)
134 [would lead to a cooling of about 1 °C after several years \(WMO, 2022\)](#). This is consistent with
135 [observed surface cooling after large volcanic eruptions, such as the 1991 Mt Pinatubo eruption which](#)
136 [produced cooling of about 0.3 °C over a 2-3 year period \(e.g., IPCC, 2021\)](#).

137
138 Many global climate models have simulated SRM in the form of stratospheric aerosol intervention
139 (SAI). Model studies include the Stratospheric Aerosol Geoengineering Large Ensemble Project
140 GLENS (e.g., Cheng et al., 2019; Simpson et al., 2019; Abiodun et al., 2021), the Geoengineering Model
141 Intercomparison Project (Kravitz et al., 2013; Tilmes et al., 2013), as well as others (e.g., Bala et al.,
142 2008; Jones et al., 2018; Muthyala et al., 2018). Compared with global warming, SAI decreases mean
143 global precipitation (Govindasamy and Caldeira, 2000; Bala et al., 2008; Robock et al., 2008; Cheng
144 et al., 2019; Simpson et al., 2019) as well as both the intensity and frequency of precipitation extremes
145 caused by GHG-induced climate change (Tilmes et al., 2013; Muthyala et al., 2018). Dagon and Schrag
146 (2016) is a rare article that focuses on the spatial variability of runoff and soil moisture responses to
147 SRM. Although solar geoengineering weakens the global hydrologic cycle (e.g., Bala et al., 2008;
148 Tilmes et al., 2013; Ricke et al., 2023), its regional impacts are method- and strategy-dependent
149 (Ricke et al., 2023) with potentially substantial changes in the regional precipitation patterns (Ricke
150 et al., 2010; Tilmes et al., 2013; Crook et al., 2015; Dagon and Schrag, 2016, Tilmes et al., 2020). While
151 differences in temperature fields vary relatively smoothly with radiative forcing, precipitation
152 patterns are far more variable being dependent on atmosphere/ocean/land surface coupling on a
153 wide range of spatial and temporal scales. Furthermore, SAI simulations rely on many model-specific
154 details and parameterizations that tend to produce larger across-model differences than simulations
155 using simpler forms of SRM (Vioni et al., 2021). While SAI may counteract the annual-mean water
156 availability changes over land forced by GHG, it is not easy to offset the regional consequences,
157 especially in the hydrological cycle, [such as the Amazonian drying trend and its reduced precipitation,](#)
158 [evaporation, and precipitation minus evaporation \(Jones et al., 2018\)](#).

159
160 Although the MENA region and the adjacent Mediterranean region are known to be a “hot spot” for
161 climatic change (Giorgi and Lionello, 2008; Bucchignani et al 2018), little has been done on potential
162 changes in TWS across MENA especially under SRM climates. This study fills that knowledge gap and
163 explores the changes that may occur in TWS under i) a high GHG emissions scenario, ii) the same GHG
164 scenario combined with SAI designed to globally neutralize the GHG radiative forcing, and iii)

165 compares both future climates with the historical conditions (1985-2014) across the Mediterranean,
166 Middle East, and northern Africa.

167

168 **2. Data and Methods**

169 **2.1. Study Area**

170 The study area is composed of MENA and southern Europe to its north including the Caspian
171 and Mediterranean Seas. MENA covers the large region from Morocco in the west to Iran in the east,
172 containing all the Maghreb and the Middle Eastern countries from the 15⁰N to 45⁰N latitude and from
173 20⁰W to 63⁰E longitude (Fig. 1). As well as a water-stressed region, MENA, is a worldwide hot spot
174 for exacerbated extreme temperatures, aridity conditions, and drought (Giorgi and Lionello, 2008;
175 Bucchignani et al., 2018). According to the Koppen Climate Classification System (Peel et al., 2007),
176 MENA broadly has a hot and arid climate except for the coastal regions and highlands. Most of
177 northern Africa (NA) has a desert climate and 90% is covered by the Saharan Desert. The 2 m air
178 temperature rises to 50°C in summertime while the annual mean precipitation is less than 25 mm
179 (Faour et al., 2016). The Arid Steppe climate predominates in Morocco, Algeria and Tunisia with cold
180 winters (Faour et al., 2016) except for the Atlas Mountains which are cooler and wetter (annual mean
181 precipitation of ~500mm).

182

183 Across the Middle East, the largest amount of precipitation falls in four main regions: the
184 coastal eastern Mediterranean Sea, the south coast of the Caspian Sea, the western sides of the Zagros
185 Mountains across Iran and Iraq, and the southern tip of the Arabian Peninsula. The Middle East also
186 contains several major deserts having little to no precipitation: the Lut and Kavir deserts in ~~the south-~~
187 ~~east and north-central regions in middle and eastern~~ Iran, the Arabian Desert, the Syrian Desert, and
188 the Negev in south-eastern corner of the Mediterranean Sea. Middle East precipitation often
189 originates from moisture coming from the west over the Mediterranean Sea (Evans and Smith, 2006).
190 The Red Sea and the Persian Gulf are also source regions for the heaviest precipitations across the
191 area.

192

193 The Mediterranean area ~~is also projected to be highly sensitive to global warming~~
194 ~~(Schleussner et al., 2016), particularly regarding water availability (Lionello et al., 2006).~~ It has mild
195 wet winters and warm to hot, dry summers as well as a complicated morphology, owing to the many
196 steep orogenic structures, distinct basins and gulfs, along with islands and peninsulas of various sizes
197 (Lionello et al., 2006).

198

199

200

201

202

203

204

205

206

207

208

209

210

211

212

213

214

215

216

217

218

219

220

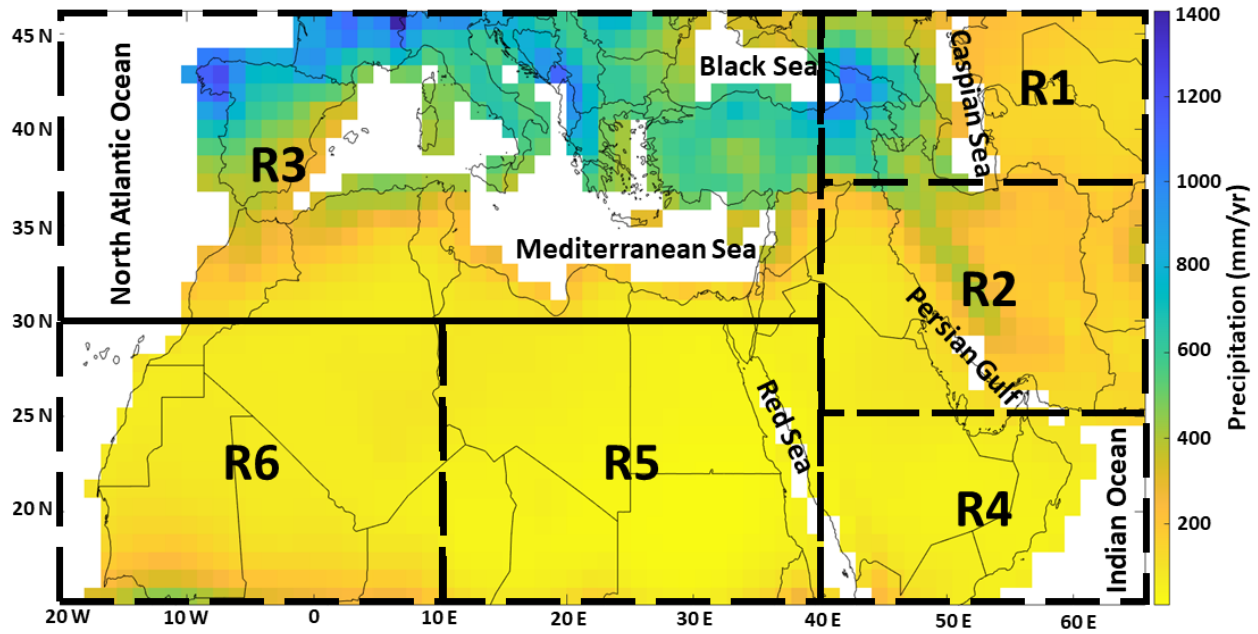
221

222

Based on its full range of climate types, we divided the study area into six sub-regions (R1 to R6) to explore the changes in hydroclimate variables under both global warming and SAI scenarios (Fig. 1). The regions R1 to R6 respectively refer to the lands around the Caspian Sea, eastern Middle East (largely containing Iran and Iraq), Mediterranean area, Arabian Peninsula, eastern NA, and western NA. The simulated present-day climatology (1985-2014) of each region for different hydrological quantities is summarized in Table 1. ~~The climatology of each region is summarized in Table 1.~~ Potential evapotranspiration (ET) is the amount of evaporation that would occur if a sufficient water source were available. The Thornthwaite method was used to calculate the potential ET based on the monthly mean temperature and latitude data for each grid. Evaporation from both soil and canopy and transpiration are summed up to obtain the real ET, which is the quantity of water actually removed from a surface by evaporation and transpiration. The lands around the Caspian and Mediterranean Seas with a cooler climate, have the highest precipitation and real ~~evapotranspiration~~ ET (ET, the quantity of water actually removed from a surface by evaporation and transpiration) while more continental eastern NA with hyper-arid climate (with annual precipitation less than 100 mm) has the lowest precipitation, real ET, soil moisture, and TWS. The lands around the Caspian Sea have the highest soil moisture and TWS. More continental refers to an area with characteristics that are typical of continental climates and is less influenced by the moderating effects of nearby oceans.

Table 1. The medians of precipitation, temperature, real evapotranspiration (ET), soil moisture, terrestrial water storage (TWS), and potential ET over each region (R1 to R6, see Fig. 1) during the historical period according to the model outputs. The results for global warming and SAI are further shown in Table S1.

Region	R1	R2	R3	R4	R5	R6
Precipitation (mm/yr)	321	182	479	78	48	112
Temperature (°C)	14.2	20.5	17.2	27.0	23.7	25.3
Real ET (mm/yr)	419	187	388	72	50	112
Soil moisture (Kg/m ²)	1846	1771	1572	1353	1155	1287
TWS (Kg/m ²)	2091	1776	1623	1348	1167	1313
Potential ET (mm/yr)	74	123	74	210	143	185



223

224 **Figure 1.** The MENA’s annual precipitation map during the historical period. Regions R1 to R6
 225 largely refer to the lands around the Caspian Sea, the eastern Middle East (largely containing Iran
 226 and Iraq), the Mediterranean area, Arabian Peninsula, eastern North Africa (NA), and western NA,
 227 respectively.
 228

229 **2.2. Model simulations and scenarios**

230 We examined the data from the NCAR Community Earth System Model version 2- Whole Atmosphere
 231 Community Climate Model Version 6 (CESM2(WACCM6)) that simulated the ~~Coupled Model~~
 232 ~~Intercomparison Project phase 6~~ (CMIP6; (Eyring et al., 2016) scenarios. CESM2 ranks among the top
 233 nine models known for their accuracy in simulating global precipitation patterns, based on the
 234 Hellinger distance metric, which compares the bivariate empirical densities of CESM2 with those of
 235 34 CMIP6 models, against historical precipitation data sourced from the Global Precipitation
 236 Climatology Centre (GPCC) (Abdelmoaty et al., 2021). CESM2 has precipitation biases about 20%
 237 lower than CESM1 (Danabasoglu et al., 2020). CESM2(WACCM6) has an interactive stratospheric
 238 aerosol treatment (Danabasoglu et al., 2020) that is consistent with observations (Mills et al., 2016).
 239 For global terrestrial ET, the CESM2(WACCM6) ranked as the second-best model among 19 CMIP6
 240 models (Wang et al., 2021). Furthermore, CESM2(WACCM6), reproduced the observed global land
 241 carbon trends remarkably well (Danabasoglu et al., 2020), and includes a full ocean model (Parallel
 242 Ocean Program version 2, POP2) to simulate the response of stratospheric aerosol change in the
 243 climate.
 244

245 CESM2 also demonstrates satisfactory performance in simulating historical climate conditions
246 within the study area. In the evaluation by Babaousmail et al. (2021), which assessed 15 CMIP6
247 models in replicating monthly rainfall patterns spanning from 1951 to 2014 in NA, CESM2(WACCM6)
248 emerged as one of the top-performing models. It accurately captured rainfall peaks across the region,
249 albeit with a slight overestimation (ranging from 5 to 10 mm/month) in the southern areas and a
250 slight underestimation (ranging from 0 to 20 mm/month) in the northern regions. Despite these
251 minor deviations, CESM2(WACCM6) was recognized as one of the models for well simulating
252 precipitation patterns across NA, achieving a Taylor skill score of 0.62. Evaluation of
253 CESM2(WACCM6) across the Mediterranean coasts placed it at the 9th and 17th positions out of 31
254 CMIP6 models for its performance in simulating temperature and precipitation (Bağçacı et al., 2021).
255 Furthermore, when it comes to simulating precipitation relative to observational data for
256 northeastern Iran during the period of 1987-2005, CESM2 stood out as the top-performing model
257 among six CMIP6 models (Zamani et al., 2020). Assessing the representation of spatial and temporal
258 variations in historical precipitation from 1980 to 2014 across Africa and the Arabian Peninsula, the
259 CMIP6 multi-mean ensemble (inclusive of CESM2(WACCM6)) demonstrated reasonable
260 performance, as highlighted in Nooni et al. (2023).

261

262 The SAI simulation we use (SSP5-8.5-SAI) is designed to employ SAI together with the high GHG
263 emissions scenario, SSP5-8.5 with the target of limiting the mean global temperatures to 1.5°C above
264 the pre-industrial (1850–1900) conditions (Tilmes et al., 2020). Under SSP5-8.5 forcing, Tilmes et al.
265 (2020) projected this threshold is exceeded around the year 2020 in CESM2(WACCM6). The
266 atmospheric component of CESM2(WACCM6) has a resolution of 1.25° in longitude and 0.9° in
267 latitude. The experiment injects SO₂ at 180° longitude at four predefined latitudes (30°N, 30°S, 15°N,
268 and 15°S) at around 25 km in 15°N/S and around 22 km at 30°N/S as suggested by Tilmes et al.
269 (2018), using a feedback control algorithm to maintain not just the global mean temperature, but the
270 interhemispheric and equator-to-pole temperature gradients (Tilmes et al., 2020). For SSP5-8.5-SAI,
271 most of the sulfur mass was the largest aerosol volumes were injected at 15°S, modest masssome at
272 15°N and 30°S, and a small amountvery little at 30°N. We used the monthly TWS (the sum of snow
273 water equivalent and soil moisture (Wu et al., 2021)), precipitation, temperature, water evaporation
274 from soil and canopy, transpiration, and soil moisture, and leaf area index (LAI) data from all five
275 ensemble members (r1 to r5) of the SSP5-8.5 scenario and the three available ensemble members
276 (1-3) of SSP5-8.5-SAI. The results for variables other than TWS are shown in the Supplementary
277 Information. For the historical period, we also used all three available realizations (r1 to r3) from

278 CESM2(WACCM6). For the anomaly analysis relative to historical conditions and ~~in turn~~, the
 279 multiple linear regression models, we used the first three ensembles of SSP5-8.5, consistent with the
 280 three available historical members. We compare the GHG and SAI scenarios over 2071-2100 with the
 281 1985-2014 historical period.

282

283 We focused on the historical period from 1985 to 2014 rather than the entire historical dataset
 284 spanning from 1850 to 2100 for several reasons. Firstly, recent historical climate data may exhibit
 285 less uncertainty, given that additional meteorological stations with improved data quality are
 286 available to be used for model calibrations (Zhang et al., 2020). Secondly, this selected historical
 287 period offers valuable insights into the observable impacts of climate change, which are highly
 288 pertinent to present-day societal and environmental challenges. These insights are of utmost
 289 importance to policymakers and communities alike. Thirdly, the chosen historical 30-year time
 290 period aligns with the 30-year periods considered for the GHG emissions and SAI scenarios, ensuring
 291 consistency in our statistical analysis. We focus on the 2071-2100 future period because the
 292 anticipated changes in TWS driven by GHG emissions are expected to be more pronounced during
 293 this time frame (Pokhrel et al., 2021). Furthermore, the SAI forcing is strongest in the later period of
 294 the simulation and is expected to produce a more significant result.

295

296 **2.3. Return periods**

297 We are interested in climate extremes, not only changes in means. Therefore, we examine how the
 298 frequency of events of some particular levels are likely to change under different scenarios. We use
 299 the generalized extreme value (GEV) distribution function to estimate the probability distribution
 300 function of the TWS extremes. A return period is an estimated average time between events such as
 301 floods or river discharge flows. It is calculated by generating the 95% normal-approximate
 302 confidence intervals in accordance with the mean and variance of the variable (here TWS).

303 The GEV probability density and cumulative distribution functions ~~is~~ are defined as (Gilleland, 2020):

$$304 \quad g(z) = \frac{1}{\sigma} t(z)^{1+\xi} e^{-t(z)}; \quad G(z) = e^{-t(z)}; \quad t(z) = \begin{cases} \left\{ 1 + \xi \left(\frac{z-\mu}{\sigma} \right) \right\}^{-1/\xi}, & \xi \neq 0 \\ e^{-\left(\frac{z-\mu}{\sigma} \right)}, & \xi = 0 \end{cases} \quad (1)$$

305 For $\xi \neq 0$, we have $t(z)^{1+\xi} = \left\{1 + \xi \left(\frac{z - \mu}{\sigma}\right)\right\}^{-(1+1/\xi)}$ and for $\xi = 0$, the x domain restricted to

306 $\xi \left(\frac{z - \mu}{\sigma}\right) > -1$ where $\left(\cdot\right)_+$ denote that the value inside the bracket is set to zero when < 0 . The GEV

307 distribution is parameterized using ξ , μ , and σ which are the shape, location, and scale parameters,
 308 respectively and analogous to the skewness, mean and standard deviation. We assume that the GEV
 309 is the valid distribution function for variables z_1, \dots, z_n representing the annual maximum return
 310 TWS levels, where the quantiles of the distribution function give the return levels, z_p . The return
 311 levels are the solutions to $G(z_p) = 1 - p$, which yields (Gilleland, 2020):

$$312 \quad z_p = \begin{cases} \mu - \frac{\sigma}{\xi} [1 - \{-\ln(1-p)\}]^{-\xi} & \text{for } \xi \neq 0 \\ \mu - \sigma \ln\{-\ln(1-p)\} & \text{for } \xi = 0 \end{cases} \quad (2)$$

313 p is probability corresponding to z_p . The return period is obtained as:

$$314 \quad \text{return period } (i) = 1 / (1 - \text{cdf}(i)) \quad (3)$$

315 where cdf is the cumulative distribution function. We also calculated the 95% asymptotic lower and
 316 upper confidence intervals based on the Kolmogorov-Smirnov statistic (Doksum and Sievers, 1976).
 317 We used the concatenated TWS anomaly data for the historical period, high GHG emissions, and SAI
 318 scenarios to analyze the return periods. As an example, the relationship between empirical quantiles
 319 and model quantiles as well as the probability density versus quantiles for the regions R2 and R5 are
 320 shown in Figs. S1 and S2.

321

322 **2.4. Multiple linear regression (MLR) model**

323 We want to analyze how the primary driving climate fields (surface air temperature, precipitation,
 324 and evapotranspiration ET, and LAI (i.e., vegetation coverage)) for TWS vary spatially and among the
 325 different scenarios (Zhang et al., 2022). We use a simple multiple linear regression (MLR) model with
 326 TWS as the dependent variable (Y) for each ensemble member in each region. The following
 327 procedures were conducted:

328 i) We employed the variable clustering (VARCLUS) procedure to thoroughly assess collinearity
 329 among the variables. VARCLUS is a method that effectively segregates a set of numeric variables into
 330 disjoint or hierarchical clusters, each characterized by a linear combination of the variables within
 331 the cluster (Sarle, 1990). The criterion is that when the proportion of the variance explained by a

332 cluster is larger than 0.8, it is advisable to select one variable from that cluster. Based on the results
333 obtained from VARCLUS (Figs. S3 and S4), we made specific decisions to enhance the robustness of
334 our analysis. For instance, we identified strong correlations exceeding 0.9 between potential ET and
335 temperature (Tables S2-S13 in the Supplementary Information), as well as between soil moisture
336 and TWS in all cases (except for the eastern NA (R5) in Tables S2-S13). Consequently, we chose to
337 exclude potential ET and soil moisture from our analysis due to their high levels of correlation with
338 temperature and TWS, respectively.

339

340 ii) We considered a linear regression model with potential independent variables (X): temperature,
341 precipitation, ~~and real ET, and LAI.~~ We conducted a temporal autocorrelation analysis on all the
342 variables, including temperature, precipitation, real ET, and LAI data for each model. This analysis
343 was carried out using the Autocorrelation function at a 95% confidence level. In all regions (except
344 R4), the autocorrelation results indicated that the lags at the first and second months were
345 statistically significant, while the third month lag was almost non-significant. Therefore, we modified
346 the LMS model to include information from the two preceding months in these regions. However, in
347 region R4, we observed different patterns. In this region, both real ET and temperature significantly
348 depended on their respective conditions from the two previous months, while precipitation did not
349 show this effect. Moreover, LAI in R4 exhibited dependencies on the first three and four preceding
350 months under the SSP5-8.5 and SSP5-8.5-SAI scenarios, respectively. Consequently, we incorporated
351 specific lagged months for each variable in R4.

352 ~~We excluded soil moisture in X since its variability is highly correlated with TWS changes (Fig. S2 in~~
353 ~~the Supplementary Information), so not an independent variable. Similarly, potential ET (that is the~~
354 ~~amount of water that would be removed from a surface if a sufficient water source were available)~~
355 ~~was excluded from the model due to its high spatial and temporal correlation with temperature.~~

356 iii) Identifying the outliers using the Bonferroni p -values (i.e., Bonferroni correlation) and then
357 removing them. Bonferroni correlation is a modification for p -values when several dependent or
358 independent statistical tests are being accomplished concurrently on a single data set. A Bonferroni
359 correction divides the critical p -value by the number of comparisons being made (Bland and Altman,
360 1995). The number of outlier data points excluded varies from zero to 5 (over the 700 point) in the
361 36 models.

362 iv) Fitting the final model after removing the outliers. In all regions and scenarios, the MLR models
363 are statistically significant at the 95% level. The variance explained (R^2) varies from around 0.3 in

364 the dry southern MENA to 0.89 and 0.8-96 in the wetter lands around the Caspian and Mediterranean
 365 Seas.

366 iv) Assessing the relative “importance” of the variables for TWS in the final model using the
 367 Lindeman, Merenda, and Gold (LMG) method (Lindeman et al., 1980), where the fractional variance
 368 accounted for is determined as the independent variable-order average over average contributions
 369 in models of different sizes. The LMG method considers the average contributions of each variable
 370 across different model sizes and then averages these averages to provide a more robust measure of
 371 variable importance. The LMG can be defined as (Grömping, 2007):

$$372 \quad LMG(x_k) = \frac{1}{p!} \sum_{Permutation} seqR^2(\{x_k\} | r) \quad (4)$$

373 where $seqR^2(\{x_k\} | S_k(r)) = R^2(\{x_k\} \cup S_k(r)) - R^2(S_k(r))$ and

$$374 \quad R^2(S) = \frac{Model\ SS(model\ with\ regressors\ in\ set\ S)}{Total\ SS}$$

375 Orders have the same $S_k(r) = S$ summarize into a single summand, we therefore can re-write
 376 Eq. (4):

$$377 \quad LMG(x_k) = \frac{1}{p!} \sum_{S \subseteq \{x_1, \dots, x_p\} \setminus \{x_k\}} n(S)!(p - n(S) - 1)! seqR^2(\{x_k\} | S) \quad (5)$$

378 LMG has been recommended by Johnson and LeBreton (2004) and Grömping (2007) since it uses
 379 both direct effects and impacts adjusted for other regressors in the model. As the considered
 380 variables may be correlated with each other, when a new predictor is added to a model that already
 381 contains other predictors, its impact can be influenced by the presence of those other variables. The
 382 LMG method takes into account these interactions and adjusts the variable's contribution to reflect
 383 its unique impact while considering the effects of other regressors. Importance is a unitless variable
 384 and the sum of all independent variable importance's in each model equals the model's explained
 385 variance. Here we use all three ensemble members separately to estimate the robustness of the
 386 importance estimates.

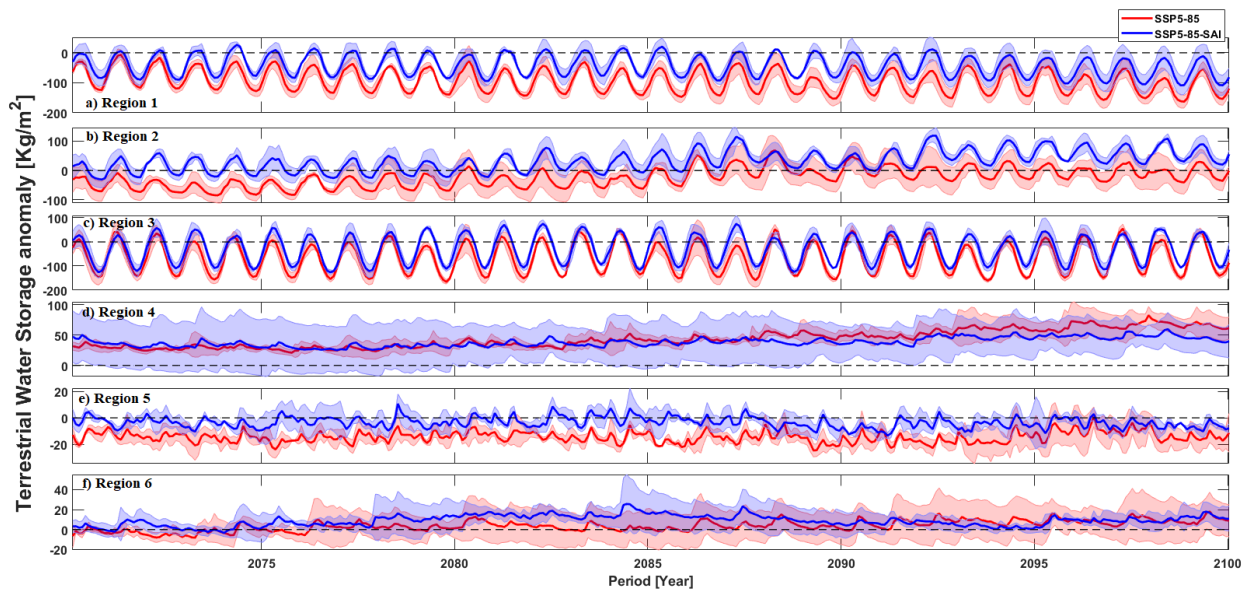
387

388 **3. Results:**

389 **3.1. Mean terrestrial water storage (TWS) changes due to GHG and SAI**

390 In this section, we present the projected changes in TWS across MENA and the lands around the
 391 Caspian and Mediterranean Seas. We discuss trends in the TWS anomalies relative to TWS averaged
 392 over the historical period (1985-2014) in response to both GHG (SSP5-8.5) forcing and to GHG+SAI.
 393 Figure 2 illustrates the original TWS anomalies, while Fig. S5 exclusively presents the long-term
 394 component, providing a clearer understanding of the changes under climate scenarios. The positive

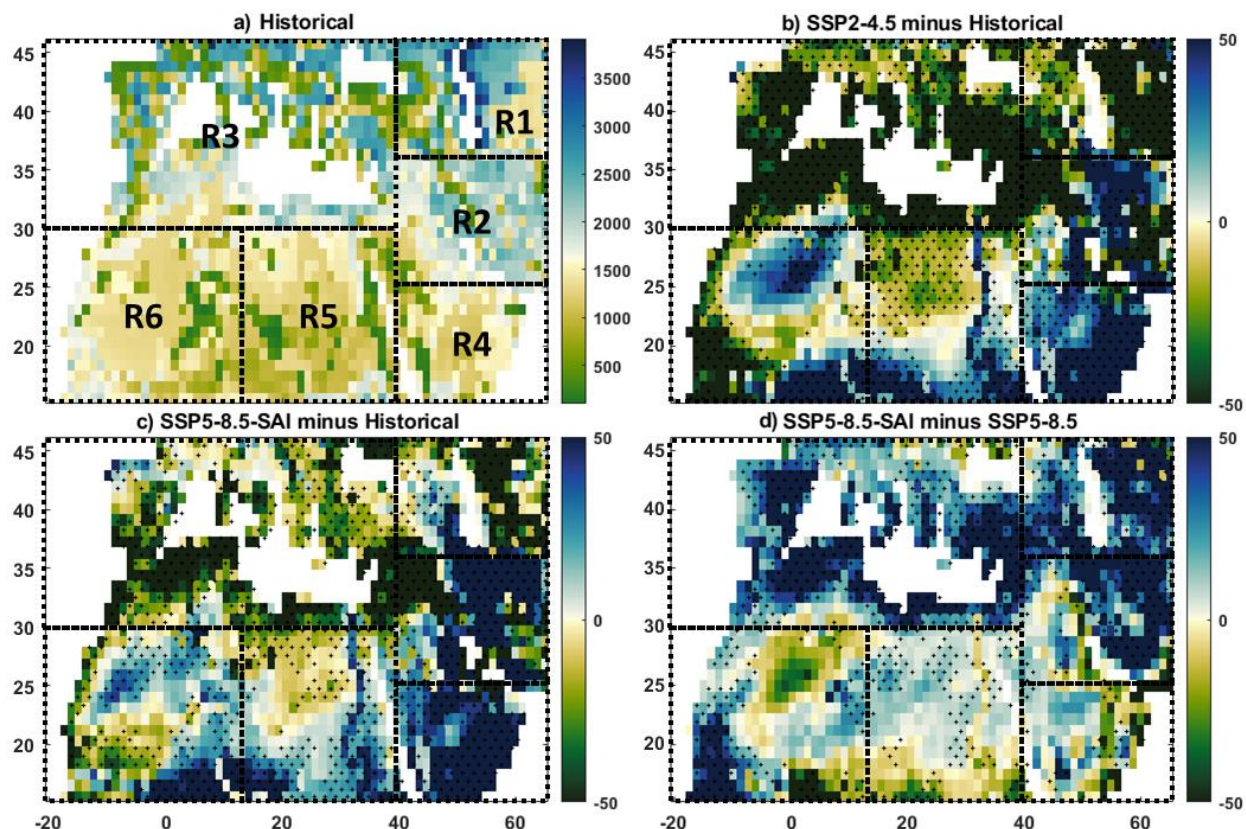
395 and negative anomalies in [these figures](#) Fig. 2 refer to increasing and decreasing TWS, respectively.
 396 The trend decreases in the northern parts (R1 and R3) and eastern NA (R5) with a hyper-arid climate
 397 but rises in the Arabian Peninsula (R4) and western NA (R6) under both GHG and SAI scenarios,
 398 particularly over the latter part of the 21st century. In all regions, the SAI climate TWS is higher than
 399 SSP5-8.5 or at least lies in the across-range of SSP5-8.5 towards the end of the century, especially in
 400 R2 and R5 (Figs. 2 and S5). ~~For R2, the TWS difference between SAI climate SAI and global warming~~
 401 ~~TWS in the region R2, particularly over the latter part of the 21st century, is greater than in relative~~
 402 ~~to the rest of the domain, particularly over the latter part of the 21st century.~~ The TWS change is
 403 smaller in the hyper-arid eastern NA (R5) than the other regions under both climate scenarios.



404
 405 **Figure 2.** The TWS anomaly relative to the TWS averaged over the historical period across MENA
 406 and the lands around the Caspian and Mediterranean Seas under global warming without (SSP5-
 407 8.5) and with SAI (SSP5-8.5-SAI). Figures a-f respectively are for regions R1 to R6. Shading in each
 408 curve shows the across-ensemble range. The dashed line crossing the y-axis at zero in each subplot
 409 is the ensemble mean of TWS over the historical period (1985-2014).

410
 411 Fig. 3 depicts the TWS differences between the historical (1985-2014) and the future climate
 412 scenarios over the 2071-2100 period. Consistent with the above findings, Figs. 3b and S46a-c show
 413 that the TWS response to GHG forcing in the wet regions around the Caspian (R1) and Mediterranean
 414 (R3) Seas is simulated as declining, while across the (semi)arid MENA region, particularly in central
 415 Iran (R2), the Arabian Peninsula (R4), and the southern portions of NA (R5 and R6), there is a positive
 416 trend. Under global warming, the largest decrease in TWS occurs around the Caspian (particularly in
 417 the east) and the Mediterranean (except for its north) while its most robust increase happens in the
 418 southern margins of NA and the eastern parts of the Arabian Peninsula. SAI (Figs. 3c and S46d, e, and

419 f) partially counteracts the changes imposed by the increased GHG emission, particularly in the
 420 wetter lands around the Caspian and Mediterranean Seas which are simulated as experiencing TWS
 421 decrease under global warming. Temporal-ensemble Mm mean TWS due to GHG forcing (Fig. 3b) is only
 422 partially reversed by SAI (Fig. 3d), and the water storage shortfall is not fully canceled out by the
 423 intervention (Fig. 3c and d). However, simulated TWS in Iran and the southern half of MENA has
 424 greater water storage under SAI relative to the historical period (Fig. 3c).
 425

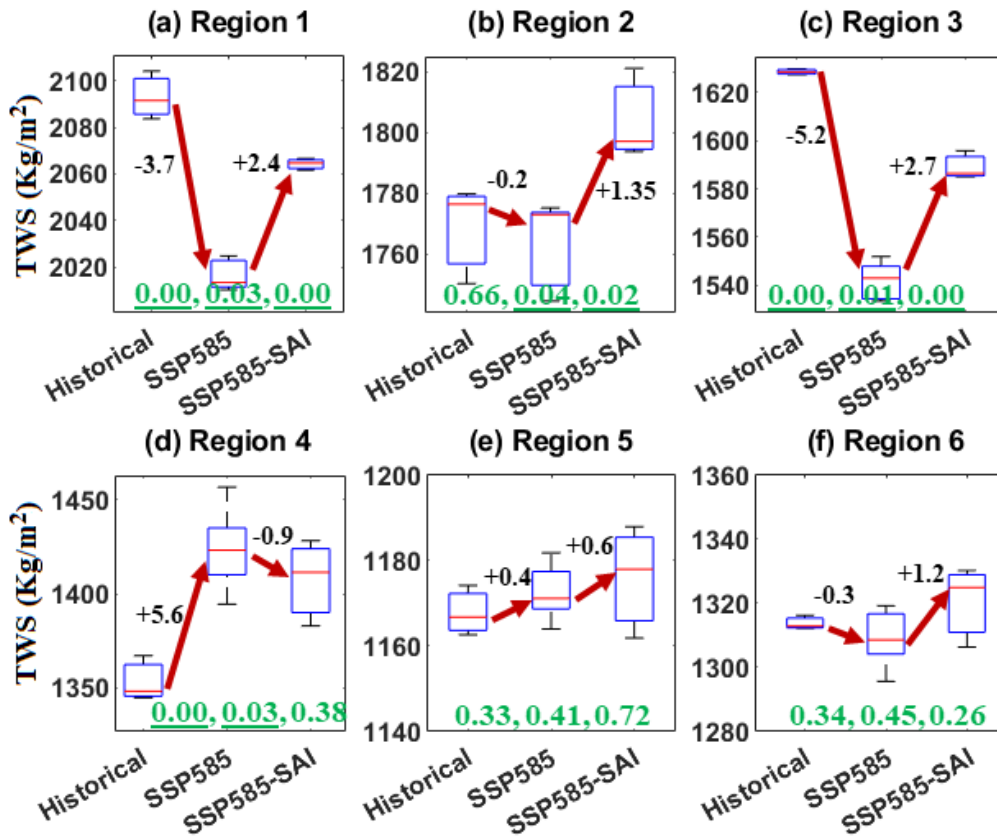


426 **Figure 3.** Ensemble mean maps of TWS across the studied domain in the historical climate (a) over
 427 1985-2014 and their projected future changes in the 2071-2100 period under the SSP5-85 GHG
 428 scenario (SSP5-8.5 minus historical (b) and GHG+SAI minus historical (c)). The extent to which the
 429 SAI impacts the TWS changes imposed by global warming is further shown (SAI minus SSP5-8.5
 430 (d)). Hatched areas show where all ensemble members agree on the sign of the changes.
 431

432
 433 In Fig. 4, we compare how simulated TWS statistical distributions vary between scenarios for each
 434 region. Mean TWS significantly ($p < 0.05$) decreases in the wetter lands around the Caspian (R1) and
 435 Mediterranean (R3) Seas to the north ($353.7-5.2\%-58 \text{ Kg/m}^2$ on area average) while it significantly
 436 increases in the dry region of Arabian Peninsula ($75 \text{ Kg/m}^2 5.6\%$) in response to GHG warming. SAI,
 437 on the whole, partially reverses the projected changes in TWS from increasing GHG concentrations

438 toward its historical values. Interestingly, SAI overcompensates the TWS changes imposed by the
 439 high GHG forcing in Iran and Iraq (R2) where this region shows no significant change under GHG
 440 emissions (Figs. 4b). SAI also has an amplifying effect in R5 and a slight overcompensation in R6, but
 441 its impact is statistically insignificant.

442
 443



444
 445 **Figure 4.** Box and whiskers plot of the changes in the Terrestrial Water Storage (TWS) in regions 1
 446 to 6 over 2071-2100 under SSP5-8.5 and SSP5-8.5-SAI relative to historical conditions (1985-
 447 2014). The titles of each subplot refer to the regions. The median for each experiment is denoted by
 448 the red line, the upper (75th) and lower (25th) quartiles by the top and bottom of the box, and
 449 ensemble limits by the whisker extents. The positive/negative values in black are the change
 450 percent under SSP5-8.5 and SSP5-8.5-SAI relative to the median of the historical period data. The
 451 three values in green refer to p-values between historical and global warming, historical and SAI,
 452 and global warming and SAI, respectively, obtained from *t*-test analysis in which the underlined *p*-
 453 values are statistically significant.

454

455 We also compared the changes in TWS with changes in precipitation, temperature, real ET, soil
 456 moisture, and potential ET over each region under both global warming and SAI scenarios (Figs. S7
 457 to S10 in the Supplementary Information). The TWS decreasing patterns under both SSP5-8.5 and
 458 SSP5-8.5-SAI scenarios across the entire study area are similar to soil moisture change patterns (Fig.

459 S7 and S9 in Supplementary Information), but are more widespread than precipitation under global
460 warming (Fig. S9). Notably, in the Mediterranean and the dry MENA region, the soil moisture
461 variability accounts for the dominant component of TWS variability (Pokhrel et al., 2021). However,
462 the decreased TWS is seen beyond the regions of reduced precipitation (Fig. S9), from beyond the
463 Mediterranean and Atlantic coasts to include Syria, Iraq, and the lands around the Caspian Sea as well
464 as to a wide portion of NA (Fig. 4). These include places where precipitation is either increasing or
465 shows no significant change, consistent with results reported by Cook et al. (2020).

466
467 In Summary, our findings show that the SSP5-8.5-SAI scenario has a potential to partially offset the
468 significant changes in mean TWS imposed by SSP5-8.5 over the entire MENA. While SAI (Fig. 3d)
469 succeeded in reversing mean TWS deficits in the wetter lands around the Caspian and Mediterranean
470 Seas driven by the GHG SSP5-8.5 scenario (Fig. 3b), it did not fully cancel out the TWS deficits (Figs.
471 3c, 4a, and 4c). However, in the dry MENA regions (Fig. 3d), particularly Iran (containing the Lut
472 desert in the south-east region and the Kavir desert in the north-central), Iraq, and the Arabian
473 Peninsula (housing the Arabian Desert), SAI resulted in higher mean water storage relative to the
474 historical period (Figs. 3c and 4).

475 476 **3.2 Changes in extreme TWS**

477 We compared changes in the expected return frequency of comparatively rare events to those during
478 the historical period. Changes in mean conditions discussed so far are clear, but the changes in
479 extremes display even larger separations between those expected under pure GHG forcing and the
480 GHG+SAI scenarios. An increase in the return level or decrease in the return period of TWS means
481 that the rare levels of high water availability increase, while a decrease in return level for a given
482 period means that rich water availability events become rarer. We applied a GEV distribution to the
483 complete dataset of monthly TWS values without explicitly setting maximum values in Fig. 5. For
484 comparison, we also extracted the annual maximum TWS values and provided the corresponding
485 fitted GEV distribution. Overall, the probability densities for both datasets exhibit a high degree of
486 similarity across various regions and scenarios (e.g., Figs. S11 and S12). Additionally, the graphs
487 depicting return levels versus return periods based on annual maximums (Fig. S13) closely resemble
488 the results obtained from the entire dataset (Fig. 5). In all cases, the trends are highly similar
489 (compare Figs. 5 and S13), although it's worth noting that the annual maximums scenario exhibits
490 slightly wider upper and lower bounds compared to the entire dataset scenario. We therefore focus
491 on the results obtained from the entire dataset. Fig. 5 shows the return levels versus return period

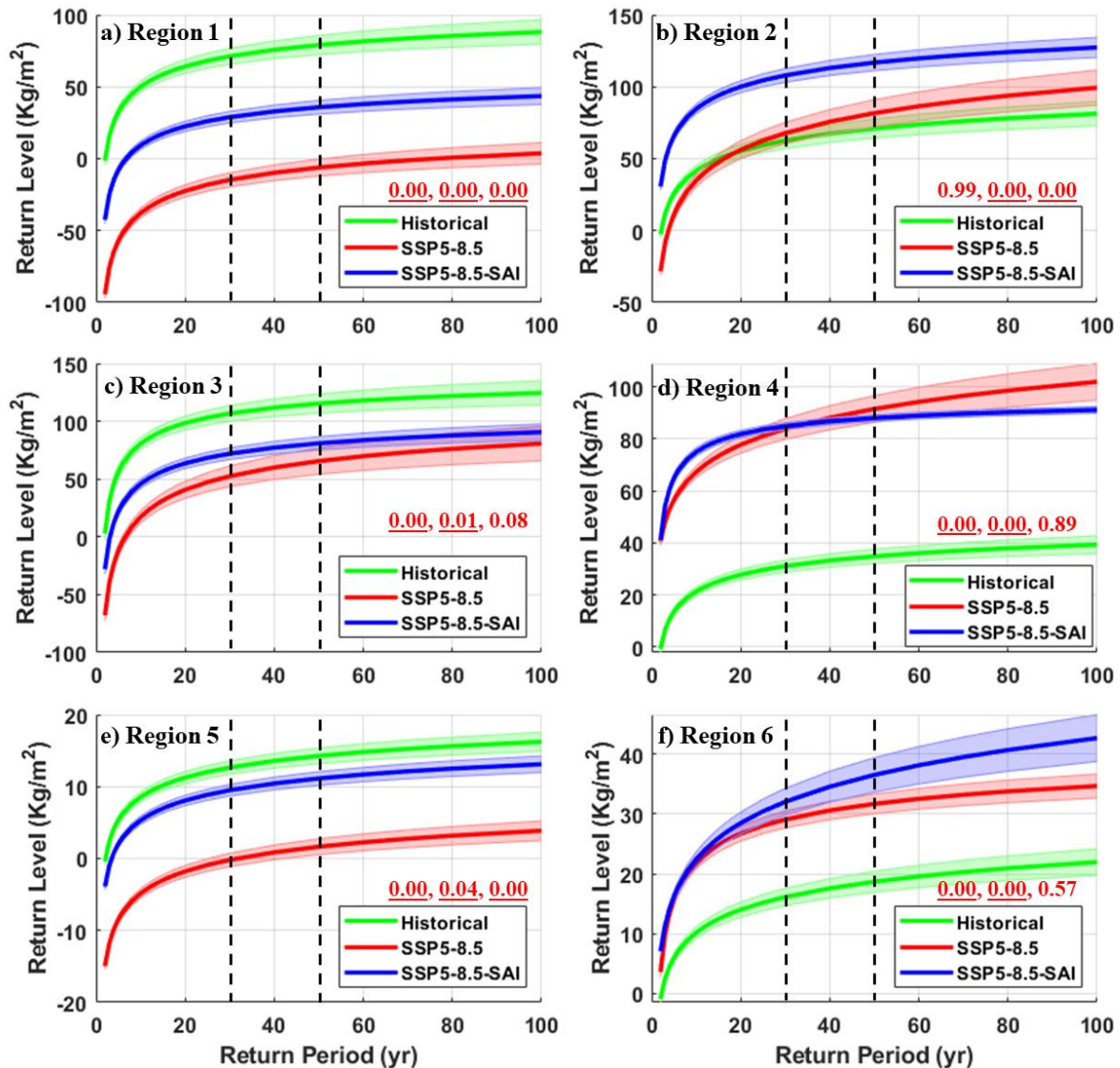
492 curves with the 95% lower and upper bands. To determine which curves (including its upper and
493 lower bounds) are significantly different from each other (p -values less than 0.05), we first conducted
494 the repeated measures analysis of variance which compares means across one or more variables that
495 are based on repeated observations, and then performed post hoc Tukey-Kramer comparisons. If one
496 curve, including its bands, does not overlap its adjacent curve, we can say that the change at that
497 return period is significant. The expected return levels versus return period curves (Fig. 5) decrease
498 in response to both GHG warming and GHG+SAI in the Caspian and Mediterranean Seas area (R1 and
499 R3) as well as in the eastern NA (R5) as a more continental dry land but increase in the Arabian
500 Peninsula (R4) and western NA (R6). In Iran and Iraq (R2), SAI leads to a significant increase in
501 expected TWS return levels ~~returns~~ relative to both historical conditions and the high GHG emission
502 scenarios (Fig. 5b). ~~While~~ SAI tends to partially counteract the GHG-driven TWS changes in R1, R3,
503 R4, and R5. Larger TWS levels are expected for the entire MENA compared with the GHG climate
504 alone, particularly in Iran, Iraq, and the western NA. Nonetheless, compared to the historical period,
505 the Arabian Peninsula (Fig. 5d) is the region with the most robust increase in the extreme TWS under
506 both the global warming and SAI scenarios. Extreme TWS in its neighbor dry land of eastern NA with
507 a hyper-arid climate is still smaller than the historical conditions.

508

509 Table 2 quantitatively compares the differences between TWS (and its corresponding 95% lower and
510 upper bounds in Fig. 5) changes at 30-, 50-, and 100-yr return periods under historical, global
511 warming, and SAI scenarios. Global warming, on the whole, decreases the TWS extremes (i.e., fewer
512 wetter conditions) at 30- to 100-year return periods over all the study areas except for the Arabian
513 Peninsula (R4) and western NA (R6). The most robust decreases in the extreme TWS imposed by
514 global warming relative to historical conditions occur in the lands around the Caspian R1 (~~-42.5~~
515 ~~Kg/m²-108%~~ on average over return periods from 30- to 100-year) and Mediterranean R3 (~~-17.6-~~
516 ~~43%Kg/m²~~ on average) and the eastern NA R5 (~~-5.71-Kg/m²-89%~~ on average) are partially
517 suppressed by SAI. A small ~~decrease~~-increase in the extreme TWS in Iran and Iraq (R2) simulated
518 under GHG (~~-2.8-Kg/m²+15%~~) is overcompensated by SAI (~~+21.0-Kg/m²+57%~~). Although SAI
519 decreases the TWS in the Arabian Peninsula (~~-2.2-Kg/m²-11%~~) relative to global warming, it still
520 tends to experience the most robust extreme water storage increases in the future (+153%)
521 compared with historical conditions. In western NA, the SAI simulation slightly intensifies the
522 increased extreme TWS imposed by high GHG emissions by +1.9 Kg/m²27%. Although SAI partially
523 compensates for the changes over most of the study area (positive SSP5-8.5-SAI minus SSP5-8.5
524 values in Table 2), on the whole, extreme TWS tend to increase in the dry regions of Iran and Iraq,

525 the Arabian Peninsula, and western NA while substantially decreasing in the wetter lands around the
 526 Caspian and Mediterranean Seas, and to lower degrees, in the eastern NA as a more continental dry
 527 land compared with historical conditions.

528



529

530 **Figure 5.** The TWS anomaly return level versus return period using the first three realizations for
 531 the historical, SSP5-8.5, and SSP5-8.5-SAI in regions 1 to 6 (a to f). The two parallel dashed black
 532 lines refer to 30- (left) and 50-year (right) return periods. Shading in each curve is the 95% upper
 533 and lower confidence bands. The three values in red refer to p-values between historical and
 534 global warming, historical and SAI, and global warming and SAI, respectively, obtained from the
 535 repeated measures analysis of variance and the post hoc Tukey-Kramer comparisons in which the
 536 underlined p-values are statistically significant.

537

538

539 **Table 2.** The percent differences (in $\text{Kg}/\text{m}^2\%$) between the medians of the TWS return level at 30-,
 540 50-, and 100-year return periods using the first three realizations for the historical, SSP5-8.5, and
 541 SSP5-8.5-SAI. Consistently, the value inside the parenthesis is the percent difference-range values
 542 between lowers and uppers 95% confidence intervals from different scenarios.

Region	(SSP5-8.5 - Historical)/Historical*100			(SSP5-8.5-SAI - Historical)/Historical*100			(SSP5-8.5-SAI - SSP5-8.5)/Historical*100		
	30-yr	50-yr	100-yr	30-yr	50-yr	100-yr	30-yr	50-yr	100-yr
R1	-121 (-130, -113)	-108 (-117, -100)	-96 (-105, -88)	-59 (-62, -57)	-55 (-57, -53)	-51 (-53, -49)	61 (56, 68)	53 (48, 60)	45 (40, 52)
R2	8 (6, 11)	15 (12, 17)	22 (20, 24)	73 (66, 81)	65 (58, 73)	57 (50, 65)	64 (55, 75)	50 (41, 60)	34 (25, 46)
R3	-51 (-56, -46)	-43 (-49, -38)	-35 (-42, -29)	-33 (-34, -32)	-30 (-31, -29)	-27 (-28, -26)	18 (14, 24)	13 (8, 20)	8 (2, 16)
R4	170 (163, 178)	163 (157, 169)	160 (155, 164)	173 (158, 191)	153 (138, 170)	132 (117, 150)	4 (-4, 13)	-10 (-19, 1)	-27 (-39, -14)
R5	-102 (-110, -95)	-89 (-96, -82)	-76 (-83, -70)	-25 (-26, -24)	-22 (-23, -21)	-19 (-20, -18)	77 (70, 84)	67 (61, 73)	57 (52, 63)
R6	80 (73, 89)	70 (63, 77)	58 (52, 65)	99 (95, 103)	95 (93, 99)	94 (93, 96)	18 (14, 22)	26 (21, 30)	36 (31, 41)

543
544

545 3.3 Drivers of TWS change

546 To assess which variables have the most impact on mean TWS under both global warming and SAI,
 547 we fitted an MLR model to each ensemble member separately in each of the six regions (Figs. 6 and
 548 7). The most important variable for the mean TWS under both global warming and SAI scenarios is
 549 region-specific. In the wet lands surrounding the Caspian (R1) and Mediterranean (R3) Seas,
 550 temperature and precipitation are the primary drivers of TWS changes. In contrast, in the Middle
 551 East, characterized by predominantly dry climates (R2 and R4), vegetation coverage (i.e., LAI) plays
 552 a dominant role. This observation aligns with the fact that temperature limits ET in the wet regions,
 553 while in arid and hot regions, the availability of water for ET is the predominant limiting factor (Bao
 554 et al., 2021). In NA, where TWS changes are irregular, temperature holds the greatest significance in
 555 the eastern regions (R5), while real ET is the primary driver in the west (R6). In lands around the
 556 Caspian Sea (R1), precipitation is the most important variable for TWS while temperature is a
 557 primary driver in lands around the Mediterranean. The real ET is the most important variable in dry
 558 regions R2, R4 to R6 under both GHG forcing (Fig. 6) and the SAI except for one case (R5 under the
 559 SAI in Fig. 7). Warmer climate enhances the atmospheric water content over regions and seasons
 560 (Cook et al., 2020) since 1°C warming is accompanied by ~7% enhancement in the air water storage
 561 capacity (Trenberth, 2011), and, in turn, increases the evaporative demand (Arnell, 1999), and vice
 562 versa for cooler conditions. Real ET itself is mostly controlled by temperature and available water for

563 evaporation (i.e., precipitation, soil moisture, and vegetation coverage). With just temperature and
564 precipitation as independent variables, we find that the temperature under both global warming and
565 SAI is generally more important for TWS than precipitation over the wet lands around the Caspian
566 and Mediterranean ~~wet Seas as well as the eastern NA region due to evapotranspiration~~. In contrast,
567 precipitation plays a stronger role on TWS in Iran, Iraq, and the western NA lands around the Caspian
568 Sea with lower precipitation ~~as well as all dry regions (except for R5 under SAI)~~ under both future
569 climate scenarios.

570

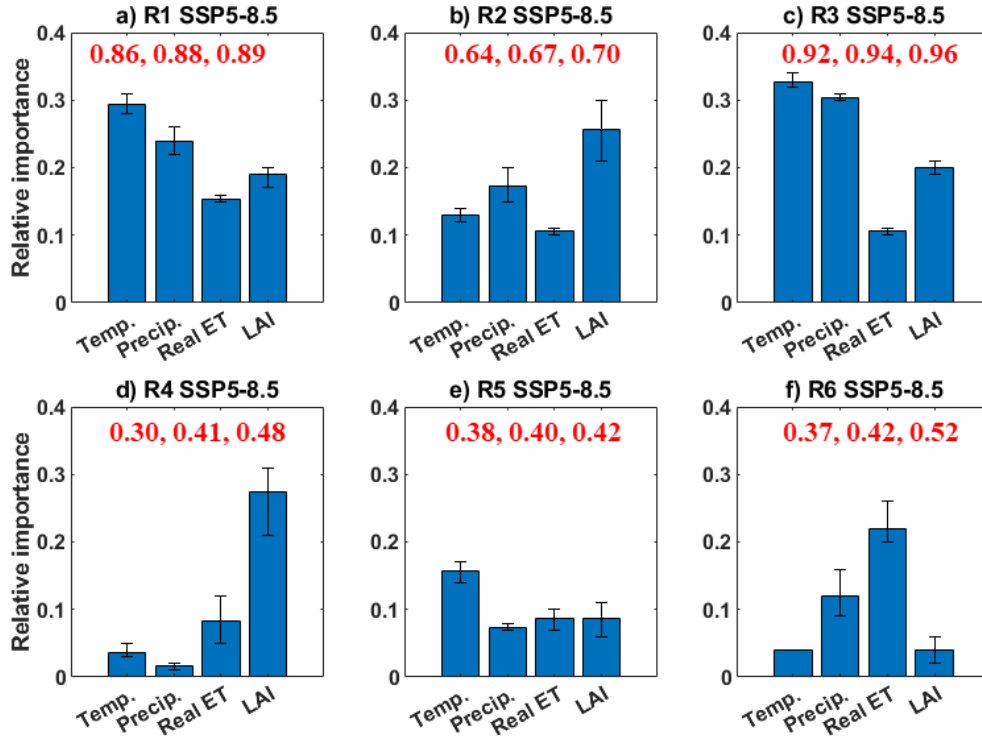
571 The regression models indicate that TWS is mostly driven by the combined impacts of changes in
572 vegetation coverage, real ET, ~~both~~ temperature and precipitation, consistent with the fact that
573 precipitation is not the only controlling factor for water resources (Cook et al., 2014; Wu et al., 2020).
574 However, the temperature in the Mediterranean area with the highest precipitation over the entire
575 domain studied plays a more important role than ~~both precipitation, vegetation coverage, and~~ real
576 ETV ~~and precipitation~~ under both warming and SAI scenarios.

577

578 Caution is required when interpreting the relative importance results for the arid regions of R4 to R6
579 as their variance explained ($R^2=0.3$ to 0.4552) from the MLR models is smaller than those (up to 0.89
580 and 0.896) for the wetter lands around the Caspian and Mediterranean Seas. This, most probably,
581 arises from the arid to hyper-arid climate of R4 to R6 with a small and irregular annual precipitation,
582 and, in turn, irregular TWS anomaly time series (Figs. 2d, e, and f).

583

584



585

586

587

588

589

590

Figure 6. LMG importance plot (Lindeman et al., 1980) of the ~~three~~four independent variables in the regression for TWS for the global warming SSP5-8.5 scenario in each region. The bar and range-bar respectively show the ensemble mean importance and the range of importance from the three ensemble members. The three values in red on each subplot shows the minimum, mean, and maximum variances explained by models.

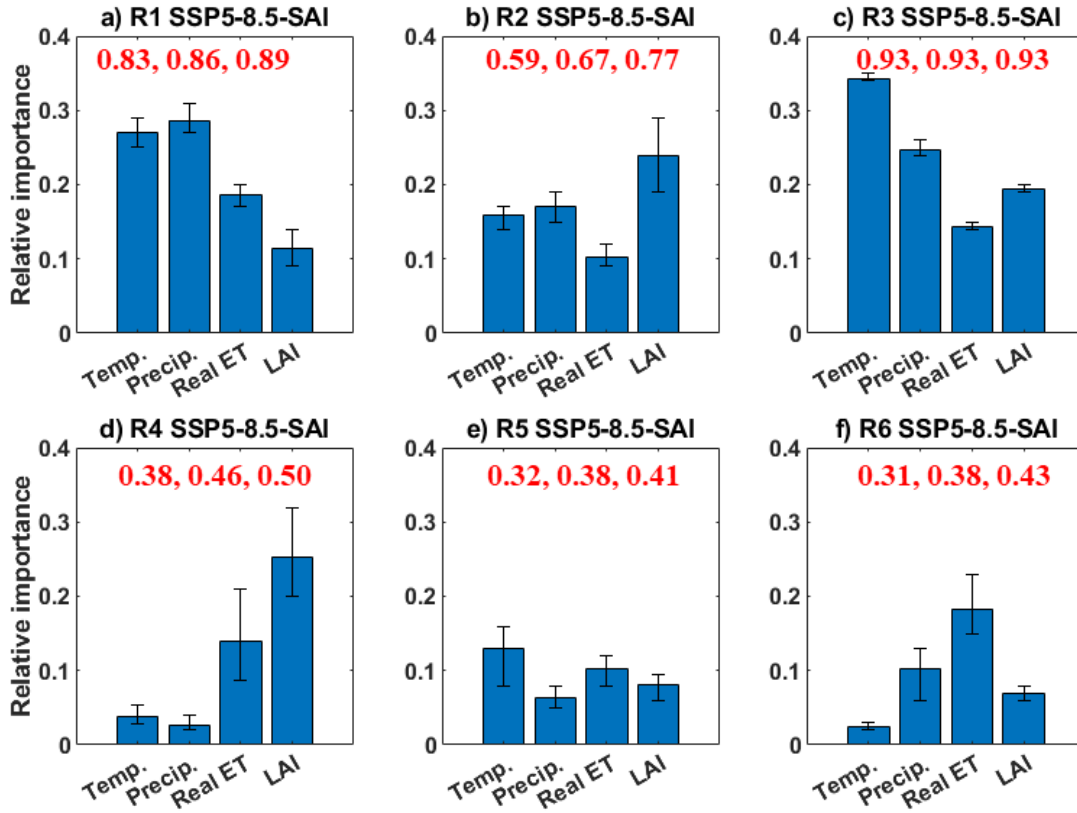


Figure 7. As in Fig. 6, but for the SSP5-8.5-SAI scenario.

591

592

593

594 4. Discussion

595 We have analyzed the potential impacts of the unmitigated global warming SSP5-8.5 scenario (GHG)
 596 and the same GHG emissions trajectory with the addition of SAI (GHG+SAI) on both the mean and
 597 extreme water storage across the lands around the Caspian and Mediterranean Seas, Middle East,
 598 and NA. We have used the CESM2(WACCM) climate model simulations with three realizations of each
 599 historic and SSP5-8.5-SAI scenario and five available realizations for SSP5-8.5. In response to high
 600 GHG emission over the 2071-2100 period, the mean TWS decreases in the wetter regions (i.e., around
 601 the Caspian and Mediterranean Seas with mild wet winters and warm to hot, dry summers), in
 602 agreement with the previous studies based on SSP5-8.5 (e.g., Cook et al., 2020; Scanlon et al., 2023),
 603 RCP2.6 and RCP4.5 (e.g., Döll et al., 2018) as well as with projections from 11 global hydrological
 604 models (Schewe et al., 2014) with globally forced 2°C warming (Schleussner et al., 2016). Similarly,
 605 a decrease in precipitation (Kim and Byun, 2009), surface runoff (Cook et al., 2020), and TWS
 606 (Pokhrel et al., 2021) has been reported across Mediterranean coasts under GHG warming. In
 607 contrast, while, on the whole, the mean TWS ~~it~~ increases or shows no significant change in the ~~dry~~
 608 areas of MENA, housing several major deserts with minimal precipitation. The temporal-ensemble

609 mean TWS increase in the southern MENA is consistent with other climate model simulations
610 showing increased precipitation and soil moisture in CMIP6 simulations under SSP5-8.5 (Cook et al.,
611 2020), and SSP2-4.5 (Ajjur et al., 2021; Scanlon et al., 2023). This further aligns with a projected
612 northward shift of the inter-tropical convergence zone (ITCZ) in eastern Africa, mostly during a
613 months of May to October (Mamalakis et al., 2021), leading to increased moisture transfer to the
614 Southern Middle East and NA (Waha et al., 2017). ~~The decrease in mean TWS in the Mediterranean~~
615 ~~projected under the global warming SSP5-8.5 with CESM2(WACGM) here is also in agreement with~~
616 ~~the previous studies based on SSP5-8.5 (e.g., Cook et al., 2020; Scanlon et al., 2023), RCP2.6 and~~
617 ~~RCP4.5 (e.g., Döll et al., 2018). It is also consistent with projections from 11 global hydrological~~
618 ~~models (Schewe et al., 2014) with globally forced 2°C warming (Schleussner et al., 2016).~~

619

620 ~~The SSP5-8.5-SAI scenario tends to reverse, to a degree, the significant changes in mean TWS~~
621 ~~imposed by SSP5-8.5 over the entire MENA. Although the decreased TWS in the wetter lands around~~
622 ~~the Caspian and Mediterranean Seas driven by the GHG SSP5-8.5 scenario (Fig. 3b) was partially~~
623 ~~reversed by the SAI (Fig. 3d) here, the mean TWS deficit is not fully canceled out by the intervention~~
624 ~~(Figs. 3c, 4a, and 4c). However, SAI causes the dry MENA regions (Fig. 3d), particularly Iran, Iraq, and~~
625 ~~the Arabian Peninsula, to have higher mean water storage relative to the historical period (Figs. 3c~~
626 ~~and 4).~~

627

628 ~~Since~~ Given the prevailing water scarcity challenges in most parts many regions of the Middle East
629 where population growth is a continuing concern (Oroud, 2008) already suffer from water shortage,
630 by mitigating the vulnerability to global warming, SAI appears to improvemay offer a potential
631 strategy toe augment the regional water status-resources across the area, particularly in the dry
632 regions of Iran, ~~(containing the Lut desert in the south-east region and the Kavir desert in the north-~~
633 central), Iraq, and the Arabian Peninsula (housing the Arabian Desert), as compared with the pure
634 GHG forced scenario. ~~Similarity, Jones et al. (2018) found that SAI could effectively counteract the~~
635 changes in available water imposed by global warming on Earth's lands.SAI may decrease the
636 vulnerability of the region to changing climate conditions. This is important in the context of
637 substantial population growth during the past half a century which is expected to continue albeit at
638 a lower rate (Oroud, 2008). Mousavi et al. (2023) also found increased soil moisture and enhanced
639 vegetation coverage would lead to the reduction of dust concentration in the MEAN region under SAI.

640

641

642 The more robust and widespread deficit in mean TWS compared to precipitation in the area, which
643 is in line with results reported by Cook et al. (2020), highlights the profound roles that other
644 variables/processes have on the increased ET such as greater atmospheric moisture demand (Dai et
645 al., 2013, 2018) and greater vegetation water use (Mankin et al., 2019) owing to warmer conditions
646 under global warming, consistent with regression model results. According to MLR model results
647 (Figs. 6 and 7), the projected changes in TWS were not solely attributable to precipitation; its
648 interplay with other factors, such as vegetation coverage, temperature, and ET play a pivotal role.
649 The vegetation coverage as the primary variable influencing changes in TWS in the MENA region
650 substantially increases under global warming (Figs. S14 and S15). It has an important, but often
651 complex and uncertain, role in surface water content (Lemordant et al., 2018; Trugman et al., 2018);
652 the denser vegetation coverage, the higher evapotranspiration rates. Furthermore, although
653 precipitation over a broad portion of MENA is lowered under SAI relative to global warming, the
654 mean TWS, in general, increases across a broad portion of the MENA region in response to the
655 intervention. TWS significantly increases over Iran and Iraq under SAI compared to historical and
656 global warming (Fig. 4b) as gains in available water from decreased temperature and, in turn, ETV is
657 largely sufficient to compensate for decreased precipitation (Figs. S3-S8 and S5-S10), signifying that
658 in addition to precipitation, the water storage also strongly depends on local temperature (Ajur et
659 al., 2021). As an example, around the Caspian Sea (R1), although the changes in precipitation imposed
660 by global warming are simulated to have been fully restored by SAI, the temperature has not; and in
661 turn, the TWS is not fully restored by SAI. This is consistent with MLR model results (Fig. 7a) in which,
662 beyond the precipitation, temperature also plays an important role in TWS across R1. Other studies
663 also found that changes in precipitation does not necessarily correlate with changes in surface water,
664 due to differences in precipitation and evaporation responses under SAI (Irvine et al., 2016).

665
666 Our findings, on the whole, suggest that the specific SAI scenario considered here could help water
667 storage in the dry regions (R2, R4, R5, and R6), i.e., leads to higher soil moisture and TWS compared
668 with both the historical conditions and pure GHG-induced global warming. Likewise, Dagon and
669 Schrag (2017) documented a rise in mean water availability and soil moisture during a period of June
670 to August in MENA using SolarGeo simulations, consistent with the significant reduction in daily
671 maximum temperatures and ET across the Middle East. This works through the combined positive
672 effects of (1) a substantial decrease in temperature and ET over the entire study area compared with
673 SSP5-8.5 global warming, and (2) the increased precipitation in the southern MENA dry regions
674 relative to historical conditions. The Middle East may therefore benefit from the water enrichment

675 from climate change through the implementation of solar intervention (Burnell, 2021). However, the
676 wet and colder regions, particularly around the Mediterranean coasts, may have less water storage
677 compared with the historical period but more water relative to the GHG scenario due to a significant
678 decrease in evapotranspiration-ET under SAI. -Simpson et al. (2019) also reported a noteworthy
679 decline of 18.5% in available water (precipitation minus evaporation) across the Mediterranean area
680 under high GHG emissions while it has been partially reversed (only 5%) by a decrease in
681 evaporation under SAI.

682
683 ~~Based on the return level period analyses, the extreme ends of the TWS probability distribution~~
684 ~~changes (Fig. 5 and Table 2) due to SAI are significant relative to both the historical period and global~~
685 ~~warming, except in one case (in R3 compared to global warming (Fig. 5c)), particularly in the lands~~
686 ~~around the Caspian and Mediterranean Seas and the Arabian Peninsula where the global warming-~~
687 ~~imposed changes are large. SAI significantly reverses the decreased extreme TWS in the northern~~
688 ~~lands of the domain as well as having enhanced extreme TWS across the Arabian Peninsula.~~
689 ~~Moreover, in the dry regions of Iran and Iraq (R2) and western NA (R6), SAI significantly increases~~
690 ~~the extreme TWS relative to both the historical conditions and global warming (Figs. 5b and 5f and~~
691 ~~Table 2). In contrast, in the hyper-arid region of eastern NA, although SAI compensates for the~~
692 ~~decreased extreme TWS, it is still smaller than the historical conditions.~~

693
694 ~~The extreme TWS under the high GHG emission scenario significantly decreases over the land around~~
695 ~~the Caspian (-42.5 Kg/m² on average over return periods from 30 to 100-year) and Mediterranean~~
696 ~~(-17.6 Kg/m² on average) as well as eastern NA (-5.71 Kg/m² on average) but increases in the dry~~
697 ~~regions of the Arabian Peninsula (+25.7 Kg/m²) and western NA (+4.7 Kg/m²). SAI partially~~
698 ~~suppresses the changes imposed by global warming except for Iran and Iraq (R2) and the western~~
699 ~~NA (R6) where it significantly increases the extreme TWS. The extreme TWS does not show~~
700 ~~significant changes in Iran and Iraq under global warming, but SAI substantially increases the~~
701 ~~extremes relative to global warming (+24.0 Kg/m²). Although SAI partially compensates for the~~
702 ~~extreme TWS changes in most of the study area, aligning with (positive SSP5-8.5 SAI minus SSP5-~~
703 ~~8.5 values in Table 2 findings by Jones et al. (2018)), on the whole, the overall extreme TWS trend~~
704 ~~tends indicates an to increase in dry regions of Iran and Iraq, Arabian Peninsula, and western NA.~~
705 ~~Conversely, there is a while substantially decrease in extreme TWS in the wetter lands around the~~
706 ~~Caspian and Mediterranean Seas, and to lower degrees, in the eastern NA compared to historical~~
707 ~~conditions. Both future climate scenarios (SSP5-8.5 and SSP5-8.5 SAI) indicate significant changes to~~

708 ~~TWS relative to historical around the Caspian and Mediterranean Seas, Middle East, and NA which~~
709 ~~will have important hydrological consequences in terms of the drought and flood disasters. The~~
710 ~~implications of our findings under both future climate scenarios (SSP5-8.5 and SSP5-8.5-SAI) extend~~
711 ~~beyond hydrology and water resources management. Changes in TWS have significant implications~~
712 ~~for climate adaptation, flood and drought risk management, and infrastructure planning.~~ Some dry
713 areas such as Iran, Iraq, and the Arabian Peninsula are projected to receive greater extreme TWS
714 under both global warming and SAI or only SAI, and these regions have suffered historically from
715 flooding (e.g., Abbaspour et al., 2009; Ghavidel and Jafari Hombari, 2020; Dezfuli et al., 2021). The
716 significant increase in extreme TWS enhances their flood risks. Hence, governments in these regions
717 should plan for adaptations to water megastructures such as the dams on the large rivers of Karkheh
718 and Karun in western Iran and the Euphrates and Tigris in Iraq, since they have been mostly designed
719 with historical hydrology in mind.

720

721 There are several caveats and caution needed for our results. First, our findings are based on a single
722 model simulation (CESM2) and a single scenario climate scenario SSP5-8.5 with (three available
723 realizations) and without (five available realizations) SAI. Future studies should consider alternative
724 SAI scenarios to explore the sensitivity of our results to model and scenario choices. The SSP
725 scenarios include some that clearly portray undesirable futures, especially the high emissions SSP5
726 scenarios or the regional rivalry SSP3 that illustrate the danger of unchecked climate change
727 (MacMartin et al., 2022). There are more caveats for the SAI experiment used here (1) it deploys in
728 2020, therefore does not simulate any plausible future, and (2) takes into account solely the high-
729 emissions scenario SSP5-8.5 that is suitable for capturing a high “signal” compared to internal
730 variability. This is useful for understanding the science but inconsistent with present-day projections
731 of mitigation attempts (Burgess et al., 2020). However, while the signal is stronger under high GHG
732 emissions, it is plausible that the directions and patterns of response would be similar in a lower-
733 emission experiment, with the magnitude of changes roughly depending on the degree of warming
734 being suppressed by SAI (e.g., MacMartin et al., 2019).

735

736 **5. Conclusions**

737 The current study is the first attempt for understanding the influence of GHG emission and SAI
738 scenarios on both mean and extreme water storage changes over the lands around the Caspian and
739 Mediterranean Seas, Middle East, and northern Africa under global warming and SAI scenarios
740 compared to the historical 1985-2014 conditions. The mean TWS is projected to decrease across the

741 wetter lands around the Caspian and Mediterranean Seas to the north (~~3.7-5.2%~~ ~~35-58 Kg/m²~~-on
742 average) but increase over the most MENA region (up to ~~75.5 Kg/m²~~ ~~5.6%~~ over the Arabian
743 Peninsula) that has a drier climate under the high GHG forcing compared to the present-day
744 conditions.

745

746 Although the SAI tends to reverse, to a degree, the significant changes in TWS revealed by SSP5-8.5
747 over the entire area, it significantly overcompensates for the slightly reduced TWS under the high
748 GHG scenario in Iran and Iraq. MLR model analysis of driving factors suggests that the impacts of
749 temperature on water storage changes, like precipitation, are also important under both high GHG
750 forcing and SAI scenarios. Although SAI mostly decreases precipitation over most of the domain, it is
751 accompanied by higher mean TWS across the entire study area due to the cooler climate.

752

753 Although significant changes in the extreme TWS under high GHG emissions are reduced by SAI, the
754 changes due to both future climate changes are still large relative to the historical period across a
755 broad portion of the domain. With SAI, TWS significantly decreases in the eastern lands around the
756 Caspian Sea while substantially increasing across the Middle East regions of Iran, Iraq, and the
757 Arabian Peninsula. This may increase flood risks since water megastructures have been mostly
758 designed with historical hydrology in mind. Finally, the SAI scenario appears to increase accessible
759 water storage in the dry regions of the Middle East and northern Africa. The wetter and colder lands
760 around the Caspian and Mediterranean Seas may have less available water compared with the
761 historical conditions, although SAI partially ameliorates the changes imposed by global warming.

762

763

764 **Data availability:**

765 The data for CESM2 simulations are publicly available via its website: [https://esgf-](https://esgf-node.llnl.gov/search/cmip6/)
766 [node.llnl.gov/search/cmip6/](https://esgf-node.llnl.gov/search/cmip6/). [To access these specific data via ESGF website use the Source ID =](#)
767 [CESM2-WACCM, Experiment ID=ssp585, and Frequency = mon. The SSP5-8.5-SAI data are freely](#)
768 [available at https://www.earthsystemgrid.org/dataset/ucar.cgd.cesm4.geomip.ssp5.html](#)
769 [\(https://doi.org/10.26024/t49k-1016\).](#)

770

771 **Acknowledgments:**

772 We appreciate the financial support from the DEGREES Initiative in collaboration with the World
773 Academy of Sciences (TWAS) under grant no. 4500443035.

774

775 **Author contributions:**

776 AR: coordinated the analysis, graphics of various figures, and manuscript preparation; KK and ST:
777 conceptualized and prepared the data; and JCM: conceptualized and coordinated the interpretation
778 and discussion for various sections. All authors contributed to the discussion and writing.

779

780 **Competingaflict ofthe Interest:**

781 The contact author has declared that none of the authors has any competing interests. There is no
782 conflict of interest.

783

784 **Financial support:**

785 This research has been supported by the DEGREES Initiative in collaboration with the World
786 Academy of Sciences (grant no. 4500443035)

787

788 **References:**

789 Abbaspour, K. C., Faramarzi, M., Ghasemi, S. S., & Yang, H. (2009). Assessing the impact of climate
790 change on water resources in Iran. *Water resources research*, 45(10).

791 Abdelmoaty, H. M., Papalexiou, S. M., Rajulapati, C. R., & AghaKouchak, A. (2021). Biases beyond the
792 mean in CMIP6 extreme precipitation: A global investigation, Earths Future, 9,
793 e2021EF002196.

794 Abiodun, B. J., Odoulami, R. C., Sawadogo, W., Oloniyo, O. A., Abatan, A. A., New, M., ... & MacMartin, D.
795 G. (2021). Potential impacts of stratospheric aerosol injection on drought risk managements
796 over major river basins in Africa. *Climatic Change*, 169(3), 1-19.

797 Ajjur, S. B., & Al-Ghamdi, S. G. (2021). Evapotranspiration and water availability response to climate
798 change in the Middle East and North Africa. *Climatic Change*, 166(3-4), 28.

799 Arjidal, K., Driouech, F., Vignon, E., Chéruey, F., Manzanas, R., Drobinski, P., ... & Idelkadi, A. (2023).
800 Future of land surface water availability over the Mediterranean basin and North Africa:
801 Analysis and synthesis from the CMIP6 exercise. Atmospheric Science Letters, e1180.

802 Arnell, N. W. (1999). Climate change and global water resources. *Global environmental change*, 9,
803 S31-S49.

804 Azzopardi, B., Balzan, M. V., Cherif, S., Doblas-Miranda, E., dos Santos, M., Dobrinski, P., ... & Xoplaki, E.
805 (2020). Climate and environmental change in the Mediterranean basin–current situation and
806 risks for the future. *First Mediterranean assessment report.*

807 [Babaousmail, H., Hou, R., Ayugi, B., Ojara, M., Ngoma, H., Karim, R., ... & Ongoma, V. \(2021\). Evaluation](#)
808 [of the performance of CMIP6 models in reproducing rainfall patterns over North](#)
809 [Africa. Atmosphere, 12\(4\), 475.](#)

810 [Bağçacı, S. Ç., Yucel, I., Duzenli, E., & Yilmaz, M. T. \(2021\). Intercomparison of the expected change in](#)
811 [the temperature and the precipitation retrieved from CMIP6 and CMIP5 climate projections:](#)
812 [A Mediterranean hot spot case, Turkey. Atmospheric Research, 256, 105576.](#)

813 Bala, G., Duffy, P. B., & Taylor, K. E. (2008). Impact of geoengineering schemes on the global
814 hydrological cycle. *Proceedings of the National Academy of Sciences*, 105(22), 7664-7669.

815 [Bao, Y., Duan, L., Liu, T., Tong, X., Wang, G., Lei, H., ... & Singh, V. P. \(2021\). Simulation of](#)
816 [evapotranspiration and its components for the mobile dune using an improved dual-source](#)
817 [model in semi-arid regions. Journal of Hydrology, 592, 125796.](#)

818 Barlow, M., Zaitchik, B., Paz, S., Black, E., Evans, J., & Hoell, A. (2016). A review of drought in the Middle
819 East and southwest Asia. *Journal of climate*, 29(23), 8547-8574.

820 Bland, J. M., & Altman, D. G. (1995). Multiple significance tests: the Bonferroni
821 method. *Bmj*, 310(6973), 170.

822 ~~[Breiman, L. \(1996\). Bagging predictors. Machine learning, 24, 123-140.](#)~~

823 Bucchignani, E., Mercogliano, P., Panitz, H.-J., & Montesarchio, M. (2018). Climate change projections
824 for the Middle East–North Africa domain with COSMO-CLM at different spatial resolutions.
825 *Advances in Climate Change Research*, 9(1), 66–80. <https://doi.org/10.1016/j.>
826 [Accre.2018.01.004](#)

827 Burgess, M. G., Ritchie, J., Shapland, J., & Pielke, R. (2020). IPCC baseline scenarios have over-projected
828 CO2 emissions and economic growth. *Environmental Research Letters*, 16(1), 014016.

829 [Burnell, L. \(2021\). Risks to global water resources from geoengineering the climate with solar](#)
830 [radiation management \(Doctoral dissertation, University of Nottingham\).](#)

831 Byun, H. R., & Wilhite, D. A. (1999). Objective quantification of drought severity and duration. *Journal*
832 [of climate](#), 12(9), 2747-2756.

833 Cook, B. I., Mankin, J. S., Marvel, K., Williams, A. P., Smerdon, J. E., & Anchukaitis, K. J. (2020). Twenty-
834 first century drought projections in the CMIP6 forcing scenarios. *Earth's Future*. 8,
835 e2019EF001461.

836 Cook, B. I., Anchukaitis, K. J., Touchan, R., Meko, D. M., & Cook, E. R. (2016). Spatiotemporal drought
837 variability in the Mediterranean over the last 900 years. *Journal of Geophysical Research:*
838 [Atmospheres](#), 121(5), 2060-2074.

839 Cook, B. I., Smerdon, J. E., Seager, R., & Coats, S. (2014). Global warming and 21 st century
840 drying. *Climate dynamics*, 43, 2607-2627.

841 Crook, J. A., Jackson, L. S., Osprey, S. M., & Forster, P. M. (2015). A comparison of temperature and
842 precipitation responses to different Earth radiation management geoengineering
843 schemes. *Journal of Geophysical Research: Atmospheres*, 120(18), 9352-9373.

844 Cheng, W., MacMartin, D. G., Dagon, K., Kravitz, B., Tilmes, S., Richter, J. H., ... & Simpson, I. R. (2019).
845 Soil moisture and other hydrological changes in a stratospheric aerosol geoengineering large
846 ensemble. *Journal of Geophysical Research: Atmospheres*, 124(23), 12773-12793.

847 Dai, A. (2013). Increasing drought under global warming in observations and models. *Nature climate*
848 *change*, 3(1), 52-58.

849 [Dagon, K., & Schrag, D. P. \(2017\). Regional climate variability under model simulations of solar](#)
850 [geoengineering. *Journal of Geophysical Research: Atmospheres*, 122\(22\), 12-106.](#)

851 [Danabasoglu, G., Lamarque, J. F., Bacmeister, J., Bailey, D. A., DuVivier, A. K., Edwards, J., ... & Strand,](#)
852 [W. G. \(2020\). The community earth system model version 2 \(CESM2\). *Journal of Advances in*](#)
853 [Modeling Earth Systems, 12\(2\), e2019MS001916.](#)

854 Dezfuli, A., Bosilovich, M. G., & Barahona, D. (2021). A dusty atmospheric river brings floods to the
855 Middle East. *Geophysical Research Letters*, 48(23), e2021GL095441.

856 Dagon, K., & Schrag, D. P. (2016). Exploring the effects of solar radiation management on water
857 cycling in a coupled land-atmosphere model. *Journal of Climate*, 29(7), 2635-2650.

858 Doksum, K. A., & Sievers, G. L. (1976). Plotting with confidence: Graphical comparisons of two
859 populations. *Biometrika*, 63(3), 421-434.

860 Döll, P., Trautmann, T., Gerten, D., Schmied, H. M., Ostberg, S., Saaed, F., & Schleussner, C. F. (2018).
861 Risks for the global freshwater system at 1.5 C and 2 C global warming. *Environmental*
862 *Research Letters*, 13(4), 044038.

863 Döll, P.; Flörke, M. Global-Scale Estimation of Diffuse Groundwater Recharge; Institute of Physical
864 Geography, Frankfurt University: Frankfurt am Main, Germany, 2005; Available online:
865 https://www.uni-frankfurt.de/45217767/FHP_03_Doell_Floerke_2005.pdf.

866 Droogers, P., Immerzeel, W. W., Terink, W., Hoogeveen, J., Bierkens, M. F. P., Van Beek, L. P. H., &
867 Debele, B. (2012). Water resources trends in Middle East and North Africa towards
868 2050. *Hydrology and Earth System Sciences*, 16(9), 3101-3114.

869 Evans, J. P., & Smith, R. B. (2006). Water vapor transport and the production of precipitation in the
870 eastern Fertile Crescent. *Journal of Hydrometeorology*, 7(6), 1295-1307.

871 Eyring, V., Bony, S., Meehl, G. A., Senior, C. A., Stevens, B., Stouffer, R. J., & Taylor, K. E. (2016). Overview
872 of the Coupled Model Intercomparison Project Phase 6 (CMIP6) experimental design and
873 organization. *Geoscientific Model Development*, 9(5), 1937-1958.

874 Fader M., Shi S., Von Bloh W., Bondeau A., Cramer W. (2016). Mediterranean irrigation under climate
875 change: More efficient irrigation needed to compensate for increases in irrigation water
876 requirements. *Hydrol. Earth Syst. Sci.* 20, 953–973. doi: 10.5194/hess-20-953-2016

877 Famiglietti, J. S. (2014). The global groundwater crisis. *Nature Climate Change*, 4(11), 945-948.

878 Faour, G., Mhaweij, M., & Fayad, A. (2016). Detecting changes in vegetation trends in the Middle East
879 and North Africa (MENA) region using SPOT vegetation. *Cybergeo: European Journal of*
880 *Geography*.

881 Fragaszy, S. R., Jedd, T., Wall, N., Knutson, C., Fraj, M. B., Bergaoui, K., ... & McDonnell, R. (2020).
882 Drought Monitoring and Warning System for the Middle East and North Africa. *Bulletin of the*
883 *American Meteorological Society*, 101(10), 904-910.

884 Ghavidel, Y., & Jafari Hombari, F. (2020). Synoptic analysis of unexampled super-heavy rainfall on
885 April 1, 2019, in west of Iran. *Natural hazards*, 104(2), 1567-1580.

886 Gilleland, E. (2020). Bootstrap methods for statistical inference. Part II: Extreme-value
887 analysis. *Journal of Atmospheric and Oceanic Technology*, 37(11), 2135-2144.

888 Giorgi, F., & Lionello, P. (2008). Climate change projections for the Mediterranean region. *Global and*
889 *Planetary Change*, 63(2-3), 90–104. <https://doi.org/10.1016/j.gloplacha.2007.09.005>

890 Giorgi F. (2006) Climate change hot-spots. *Geophys Res Lett* 33: L08707.
891 doi:10.1029/2006GL025734.

892 Govindasamy B., Caldeira K. (2000) Geoengineering Earth's radiation balance to mitigate CO2-
893 induced climate change. *Geophys Res Lett* 27:2141–2144.

894 Grömping, U. (2007). Relative importance for linear regression in R: the package relaimpo. *Journal of*
895 *statistical software*, 17, 1-27.

896 [Hobeichi, S., Abramowitz, G., Ukkola, A. M., De Kauwe, M., Pitman, A., Evans, J. P., & Beck, H. \(2022\).
897 Reconciling historical changes in the hydrological cycle over land. *npj Climate and*
898 *Atmospheric Science*, 5\(1\), 17.](#)

899 Hofste, R. W., Reig, P., & Schleifer, L. (2019). 17 countries, home to one-quarter of the world's
900 population, face extremely high water stress.

901 Intergovernmental Panel on Climate Change (IPCC): Working Group I Contribution to the Sixth
902 Assessment Report (AR6), *Climate Change 2021: The Physical Science Basis*,
903 2021, <https://www.ipcc.ch/assessment-report/ar6/> (last access: 5 December 2022), 2021.

904 [Irvine, P. J., Kravitz, B., Lawrence, M. G., & Muri, H. \(2016\). An overview of the Earth system science](#)
905 [of solar geoengineering. Wiley Interdisciplinary Reviews: Climate Change, 7\(6\), 815-833.](#)

906 Johnson, J. W., & LeBreton, J. M. (2004). History and use of relative importance indices in
907 organizational research. *Organizational research methods*, 7(3), 238-257.

908 [Jones, A. C., Hawcroft, M. K., Haywood, J. M., Jones, A., Guo, X., & Moore, J. C. \(2018\). Regional climate](#)
909 [impacts of stabilizing global warming at 1.5 K using solar geoengineering. Earth's](#)
910 [Future, 6\(2\), 230-251.](#)

911 Karami, K., Tilmes, S., Muri, H., & Mousavi, S. V. (2020). Storm track changes in the Middle East and
912 North Africa under stratospheric aerosol geoengineering. *Geophysical Research*
913 *Letters*, 47(14), e2020GL086954.

914 Kim, D. W., & Byun, H. R. (2009). Future pattern of Asian drought under global warming
915 scenario. *Theoretical and Applied Climatology*, 98(1), 137-150.

916 Konapala, G., Mishra, A. K., Wada, Y., & Mann, M. E. (2020). Climate change will affect global water
917 availability through compounding changes in seasonal precipitation and evaporation. *Nature*
918 *communications*, 11(1), 3044.

919

920 Kravitz, B., et al. (2013), An energetic perspective on hydrological cycle changes in the
921 Geoengineering Model Intercomparison Project (GeoMIP), *J. Geophys. Res. Atmos.*, 118,
922 13,087–13,102, doi:10.1002/2013JD020502

923 Lelieveld, J., Hadjinicolaou, P., Kostopoulou, E., Chenoweth, J., El Maayar, M., Giannakopoulos, C., ... &
924 Xoplaki, E. (2012). Climate change and impacts in the Eastern Mediterranean and the Middle
925 East. *Climatic change*, 114, 667-687.

926 [Lemordant, L., Gentine, P., Swann, A. S., Cook, B. I., & Scheff, J. \(2018\). Critical impact of vegetation](#)
927 [physiology on the continental hydrologic cycle in response to increasing CO2. Proceedings of](#)
928 [the National Academy of Sciences, 115\(16\), 4093. https://doi.org/10.1073/](#)
929 [pnas.1720712115.](#)

930 Lian, X., Piao, S., Chen, A., Huntingford, C., Fu, B., Li, L. Z., ... & Roderick, M. L. (2021). Multifaceted
931 characteristics of dryland aridity changes in a warming world. *Nature Reviews Earth &*
932 *Environment*, 2(4), 232-250.

933 Lindeman, R. H., Merenda, P. F., Gold, R. Z., (1980). Introduction to bivariate and multivariate
934 analysis (No. 04; QA278, L553.). Uniq ID: 5310754 Scott, Foresman, Glenview, IL.

935 Lionello, P., Malanotte-Rizzoli, P., Boscolo, R., Alpert, P., Artale, V., Li, L., ... & Xoplaki, E. (2006). The
936 Mediterranean climate: an overview of the main characteristics and issues. *Developments in*
937 *earth and environmental sciences*, 4, 1-26.

938 MacMartin, D. G., Visionsi, D., Kravitz, B., Richter, J. H., Felgenhauer, T., Lee, W. R., ... & Sugiyama, M.
939 (2022). Scenarios for modeling solar radiation modification. *Proceedings of the National*
940 *Academy of Sciences*, 119(33), e2202230119.

941 [Mamalakis, A., Randerson, J.T., Yu, J.-Y., Pritchard, M.S., Magnusdottir, G., Smyth, P. et al.](#)
942 [\(2021\) Zonally opposing shifts of the intertropical convergence zone in response to climate](#)
943 [change. 45.](#)

944 Masson-Delmotte, V., Zhai, P., Pörtner, H. O., Roberts, D., Skea, J., & Shukla, P. R. (2022). *Global*
945 *Warming of 1.5° C: IPCC Special Report on Impacts of Global Warming of 1.5° C above Pre-*
946 *industrial Levels in Context of Strengthening Response to Climate Change, Sustainable*
947 *Development, and Efforts to Eradicate Poverty*. Cambridge University Press.

948 Milly, P. C., Dunne, K. A., & Vecchia, A. V. (2005). Global pattern of trends in streamflow and water
949 availability in a changing climate. *Nature*, 438(7066), 347-350.

950 Mooney, H., Cropper, A. & Reid, W. Confronting the human dilemma. *Nature* 434, 561--562 (2005).

951 [Mousavi, S. V., Karami, K., Tilmes, S., Muri, H., Xia, L., and Rezaei, A. \(2023\). Future dust concentration](#)
952 [over the Middle East and North Africa region under global warming and stratospheric aerosol](#)
953 [intervention scenarios, Atmos. Chem. Phys., 23, 10677–10695, https://doi.org/10.5194/acp-](#)
954 [23-10677-2023](#)

955 Muthyala, R., Bala, G., & Nalam, A. (2018). Regional scale analysis of climate extremes in an SRM
956 geoengineering simulation, Part 1: precipitation extremes. *Current Science*, 1024-1035.

957 [Nooni, I.K.; Ogou, F.K.; Chaibou, A.A.S.; Nakoty, F.M.; Gnitou, G.T.; Lu, J. \(2023\). Evaluating CMIP6](#)
958 [Historical Mean Precipitation over Africa and the Arabian Peninsula against Satellite-Based](#)
959 [Observation. Atmosphere, 14, 607. https://doi.org/10.3390/atmos14030607](#)

960 Oroud, I. M. (2008). The impacts of climate change on water resources in Jordan. *Climatic changes*
961 *and water resources in the Middle East and North Africa*, 109-123.

962 Peel, M. C., Finlayson, B. L., & McMahon, T. A. (2007). Updated world map of the Köppen-Geiger
963 climate classification. *Hydrology and earth system sciences*, 11(5), 1633-1644.

964 [Pokhrel, Y., Felfelani, F., Satoh, Y., Boulange, J., Burek, P., Gädeke, A., ... & Wada, Y. \(2021\). Global](#)
965 [terrestrial water storage and drought severity under climate change. Nature Climate Change,](#)
966 [11\(3\), 226-233.](#)

967 [Ricke, K., Wan, J. S., Saenger, M., & Lutsko, N. J. \(2023\). Hydrological Consequences of Solar](#)
968 [Geoengineering. Annual Review of Earth and Planetary Sciences, 51, 447-470.](#)

969 Ricke, K. L., Morgan, M. G., & Allen, M. R. (2010). Regional climate response to solar-radiation
970 management. *Nature Geoscience*, 3(8), 537-541.

971 Reiter, L., Falk, H., Groat, C. & Coussens, C. M. (eds) *From Source Water to Drinking Water: Workshop*
972 *Summary* (National Academies Press, Washington DC, 2004).

973 Robock, A., Oman, L., & Stenchikov, G. L. (2008). Regional climate responses to geoengineering with
974 tropical and Arctic SO₂ injections. *Journal of Geophysical Research: Atmospheres*, 113(D16).

975 [Sarle, W. \(1990\). The VARCLUS Procedure. In SAS/STAT User's Guide \(fourth, Vol. 2, pp. 1641-](#)
976 [1659\). SAS Institute, Inc.](#)
977 <http://support.sas.com/documentation/onlinedoc/stat>
978 [http://support.sas.com/docu](http://support.sas.com/documentation/onlinedoc/stat)

979 Schewe, J., Heinke, J., Gerten, D., Haddeland, I., Arnell, N. W., Clark, D. B., Dankers, R., Eisner, S., Fekete,
980 B. M., ColonGonzalez, F. J., Gosling, S. N., Kim, H., Liu, X., Masaki, Y., Portmann, F. T., Satoh, Y.,
981 Stacke, T., Tang, Q., Wada, Y., Wisser, D., Albrecht, T., Frieler, K., Piontek, F., Warszawski,
982 L., and Kabat, P.: Multimodel assessment of water scarcity under climate change, *P. Natl. Acad.*
983 *Sci.*, 111, 3245–3250, doi:10.1073/pnas.1222460110, 2014

984 Shaban, A. (2008). Impact of climate change on water resources of Lebanon: Indications of
985 hydrological droughts. *Climatic changes and water resources in the Middle East and North*
986 *Africa*, 125-143.

987 Shiklomanov, I. A. & Rodda, J. C. (2003). (eds) *World Water Resources at the Beginning of the 21st*
988 *Century* (Cambridge Univ. Press, Cambridge, 2003).

989 Simpson, I. R., Tilmes, S., Richter, J. H., Kravitz, B., MacMartin, D. G., Mills, M. J., ... & Pendergrass, A. G.
990 (2019). The regional hydroclimate response to stratospheric sulfate geoengineering and the
991 role of stratospheric heating. *Journal of Geophysical Research: Atmospheres*, 124(23),
992 12587-12616.

993 Scanlon, B. R., Fakhreddine, S., Rateb, A., de Graaf, I., Famiglietti, J., Gleeson, T., ... & Zheng, C. (2023).
994 Global water resources and the role of groundwater in a resilient water future. *Nature*
995 *Reviews Earth & Environment*, 1-15.

996 Schleussner, C. F., Lissner, T. K., Fischer, E. M., Wohland, J., Perrette, M., Golly, A., ... & Schaeffer, M.
997 (2016). Differential climate impacts for policy-relevant limits to global warming: the case of
998 1.5 C and 2 C. *Earth system dynamics*, 7(2), 327-351.

999 Suppan, P., Kunstmann, H., Heckel, A., & Rimmer, A. (2008). Impact of climate change on water
1000 availability in the Near East. *Climate changes and water resources in the Middle East and*
1001 *North Africa*. Springer, Environmental Science and Engineering, Berlin.

1002 Tabari, H., & Willems, P. (2018). Seasonally varying footprint of climate change on precipitation in
1003 the Middle East. *Scientific reports*, 8(1), 4435.

1004 Tilmes, S., MacMartin, D. G., Lenaerts, J., Van Kampenhout, L., Muntjewerf, L., Xia, L., ... & Robock, A.
1005 (2020). Reaching 1.5 and 2.0 C global surface temperature targets using stratospheric aerosol
1006 geoengineering. *Earth System Dynamics*, 11(3), 579-601.

1007 Tilmes, S., Richter, J.H., Mills, M.J., Kravitz, B., MacMartin, D.G., Garcia, R.R., Kinnison, D.E., Lamarque,
1008 J.F., Tribbia, J. and Vitt, F. (2018). Effects of different stratospheric SO₂ injection altitudes on
1009 stratospheric chemistry and dynamics. *Journal of Geophysical Research:*
1010 *Atmospheres*, 123(9), pp.4654-4673.

1011 Tilmes, S., Fasullo, J., Lamarque, J. F., Marsh, D. R., Mills, M., Alterskjær, K., ... & Watanabe, S. (2013).
1012 The hydrological impact of geoengineering in the Geoengineering Model Intercomparison
1013 Project (GeoMIP). *Journal of Geophysical Research: Atmospheres*, 118(19), 11-036.

1014 Trenberth, K. E. (2011). Changes in precipitation with climate change. *Climate research*, 47(1-2),
1015 123-138.

1016 [Trugman, A. T., Medvigy, D., Mankin, J. S., & Anderegg, W. R. L. \(2018\). Soil moisture stress as a major
1017 driver of carbon cycle uncertainty. *Geophysical Research Letters*, 45, 6495–6503.
1018 <https://doi.org/10.1029/2018GL078131>](#)

1019 [Trautmann, T., Koirala, S., Carvalhais, N., Güntner, A., & Jung, M. \(2022\). The importance of vegetation
1020 in understanding terrestrial water storage variations. *Hydrology and Earth System
1021 Sciences*, 26\(4\), 1089-1109.](#)

1022 Visionsi, D., MacMartin, D. G., Kravitz, B., Boucher, O., Jones, A., Lurton, T., Martine, M., Mills, M. J., Nabat,
1023 P., Niemeier, U., Séférian, R., and Tilmes, S.: Identifying the sources of uncertainty in climate
1024 model simulations of solar radiation modification with the G6sulfur and G6solar
1025 Geoengineering Model Intercomparison Project (GeoMIP) simulations, *Atmos. Chem. Phys.*,
1026 21, 10039–10063, <https://doi.org/10.5194/acp-21-10039-2021>, 2021.

1027 [Waha, K., Krummenauer, L., Adams, S., Aich, V., Baarsch, F., Coumou, D. et al. \(2017\) Climate change
1028 impacts in the Middle East and northern Africa \(MENA\) region and their implications for
1029 vulnerable population groups. *Regional Environmental Change*, 17\(6\), 1623–1638. Available
1030 from: <https://doi.org/10.1007/s10113-017-1144-2>](#)

1031 Wang, J., Song, C., Reager, J. T., Yao, F., Famiglietti, J. S., Sheng, Y., ... & Wada, Y. (2018). Recent global
1032 decline in endorheic basin water storages. *Nature geoscience*, 11(12), 926-932.

1033 [Wang, Z., Zhan, C., Ning, L., & Guo, H. \(2021\). Evaluation of global terrestrial evapotranspiration in
1034 CMIP6 models. *Theoretical and Applied Climatology*, 143, 521-531.](#)

1035 [Wilhite, D. A., & Buchanan-Smith, M. \(2005\). Drought as hazard: understanding the natural and social](#)
1036 [context. *Drought and water crises: Science, technology, and management issues*, 3, 29.](#)

1037 World Bank (2017). *Beyond Scarcity: Water Security in the Middle East and North Africa*. The World
1038 Bank.

1039 Wu, W. Y., Lo, M. H., Wada, Y., Famiglietti, J. S., Reager, J. T., Yeh, P. J. F., ... & Yang, Z. L. (2020). Divergent
1040 effects of climate change on future groundwater availability in key mid-latitude
1041 aquifers. *Nature communications*, 11(1), 3710.

1042 [Wu, R. J., Lo, M. H., & Scanlon, B. R. \(2021\). The annual cycle of terrestrial water storage anomalies in](#)
1043 [CMIP6 models evaluated against GRACE data. *Journal of Climate*, 34\(20\), 8205-8217.](#)

1044 United Nations Educational Scientific and Cultural Organization, [UNESCO \(2003\)](#). *Water for People—*
1045 *Water for Life, The United Nations World Water Development Report* (Berghahn Books,
1046 Oxford, 2003).

1047 [Xiong, J., Guo, S., Chen, J., & Yin, J. \(2022\). Global evaluation of the “dry gets drier, and wet gets wetter”](#)
1048 [paradigm from a terrestrial water storage change perspective. *Hydrology and Earth System*](#)
1049 [*Sciences*, 26\(24\), 6457-6476.](#)

1050 [Zamani, Y., Hashemi Monfared, S. A., Azhdari Moghaddam, M., & Hamidianpour, M. \(2020\). A](#)
1051 [comparison of CMIP6 and CMIP5 projections for precipitation to observational data: the case](#)
1052 [of Northeastern Iran. *Theoretical and Applied Climatology*, 142, 1613-1623.](#)

1053 Zittis, G., Hadjinicolaou, P., Klangidou, M., Proestos, Y., & Lelieveld, J. (2019). A multi-model, multi-
1054 scenario, and multi-domain analysis of regional climate projections for the
1055 Mediterranean. *Regional Environmental Change*, 19(8), 2621-2635.

1056 Zhang, X., Li, J., Wang, Z., & Dong, Q. (2022). Global hydroclimatic drivers of terrestrial water storage
1057 changes in different climates. *CATENA*, 219, 106598.

1058 [Zhang, B., Xia, Y., Long, B., Hobbins, M., Zhao, X., Hain, C., ... & Anderson, M. C. \(2020\). Evaluation and](#)
1059 [comparison of multiple evapotranspiration data models over the contiguous United States:](#)
1060 [Implications for the next phase of NLDAS \(NLDAS-Testbed\) development. *Agricultural and*](#)
1061 [*Forest Meteorology*, 280, 107810.](#)

1062